ONE DIMENSIONAL NUMERICAL ANALYSIS OF PLASMA PROPERTIES IN THE DISCHARGE CHANNEL OF A HALL EFFECT THRUSTER

A THESIS SUBMITTED TO
THE GRADUATE SCHOOL OF NATURAL AND APPLIED SCIENCES
OF
MIDDLE EAST TECHNICAL UNIVERSITY

BY

ÇINAR YÜNCÜLER

IN PARTIAL FULFILLMENT OF THE REQUIREMENTS
FOR
THE DEGREE OF MASTER OF SCIENCE
IN
AEROSPACE ENGINEERING

SEPTEMBER 2014

Approval of the thesis:

ONE DIMENSIONAL NUMERICAL ANALYSIS OF PLASMA PROPERTIES IN THE DISCHARGE CHANNEL OF A HALL EFFECT THRUSTER

submitted by **ÇINAR YÜNCÜLER** in partial fulfillment of the requirements for the degree of **Master of Science in Aerospace Engineering Department, Middle East Technical University** by,

Prof. Dr. Canan Özgen
Dean, Graduate School of **Natural and Applied Sciences** _____

Prof. Dr. Ozan Tekinalp
Head of Department, **Aerospace Engineering** _____

Prof. Dr. Nafiz Alemdaroğlu
Supervisor, **Aerospace Engineering Dept., METU** _____

Assoc. Prof. Dr. İsmail Rafatov
Co-supervisor, **Physics Department, METU** _____

Examining Committee Members:

Prof. Dr. Yusuf Özyörük
Aerospace Engineering Department, METU _____

Prof. Dr. Nafiz Alemdaroğlu
Aerospace Engineering Department, METU _____

Assoc. Prof. Dr. İsmail Rafatov
Physics Department, METU _____

Assoc. Prof. Dr. Sinan Eyi
Aerospace Engineering Department, METU _____

Dr. Demet Uluşen
TÜBİTAK UZAY _____

Date: _____

I hereby declare that all information in this document has been obtained and presented in accordance with academic rules and ethical conduct. I also declare that, as required by these rules and conduct, I have fully cited and referenced all material and results that are not original to this work.

Name, Last Name: ÇINAR YÜNCÜLER

Signature :

ABSTRACT

ONE DIMENSIONAL NUMERICAL ANALYSIS OF PLASMA PROPERTIES IN THE DISCHARGE CHANNEL OF A HALL EFFECT THRUSTER

Yüncüler, Çınar
M.S., Department of Aerospace Engineering
Supervisor : Prof. Dr. Nafiz Alemdaroğlu
Co-Supervisor : Assoc. Prof. Dr. İsmail Rafatov

September 2014, 75 pages

The aim of this study is to understand and simulate the physical processes occurring in the discharge channel of a Hall effect thruster. Accordingly, based on a physical model proposed by A. I. Morozov, one-dimensional fluid and hybrid numerical codes are developed on Matlab software and applied to the analysis of axial distributions of plasma properties in the discharge channel of the thruster. In the hybrid model, ions are described by the kinetic Vlasov equation, while electrons and neutral atoms are treated as fluids. Initially, stationary profiles of the plasma properties are obtained. Then solving time dependent equations, time evolution of these properties is investigated. In different operating regimes, damped, periodic, and aperiodic irregular oscillations of the plasma properties are observed and discussed. The performance parameters of the thruster such as thrust, efficiency and specific impulse are estimated for different input conditions. The results obtained from fluid and hybrid models are compared.

Keywords: Hall Effect Thruster, Gas Discharge, Plasma Physics, Hybrid Model

ÖZ

HALL ETKİLİ PLAZMA İTKİ SİSTEMİNİN BOŞALMA KANALINDAKİ PLAZMA ÖZELLİKLERİNİN BİR BOYUTLU SAYISAL ANALİZİ

Yüncüler, Çınar
Yüksek Lisans, Havacılık ve Uzay Mühendisliği Bölümü
Tez Yöneticisi : Prof. Dr. Nafiz Alemdaroğlu
Ortak Tez Yöneticisi : Doç. Dr. İsmail Rafatov

Eylül 2014 , 75 sayfa

Bu çalışmanın amacı Hall etkili bir itki motorunun boşalma kanalında gerçekleşen fiziksel süreçleri anlamak ve simüle etmektir. Bu doğrultuda, A. I. Morozov tarafından önerilen bir fiziksel model temel alınarak, Matlab yazılımında bir boyutlu akışkan ve hibrit sayısal kodlar geliştirilmiş ve motorun boşalma kanalındaki plazma özelliklerinin eksenel dağılımlarının çözümlenmesine uygulanmıştır. Hibrit modelde iyonlar kinetik Vlasov denklemiyle betimlenirken elektronlar ve nötr atomlar akışkan olarak alınmıştır. İlk olarak plazma özelliklerinin durağan profilleri elde edilmiştir. Daha sonra zamana bağlı denklemler çözülerek bu özelliklerin zaman içindeki değişimleri incelenmiştir. Farklı çalışma rejimlerinde, plazma özelliklerinin sönümlü, periyodik ve düzensiz aperiyodik salınımları gözlemlenmiş ve tartışılmıştır. Motorun itki, verim ve özgül darbe gibi performans parametreleri, farklı girdi koşulları için öngörülmüştür. Akışkan ve hibrit modellerden elde edilen sonuçlar karşılaştırılmıştır.

Anahtar Kelimeler: Hall Etkili İtki Sistemleri, Gaz Deşarjı, Plazma Fiziği, Hibrit Model

To my family

ACKNOWLEDGMENTS

First, I would like to express my gratitude to my thesis supervisor Prof. Dr. Nafiz Alemdaroğlu for his guidance, encouragements and confidence in me.

I would like to thank my co-advisor Assoc. Prof. Dr. İsmail Rafatov for giving me insight into plasma physics and for his help throughout the development process of the numerical code.

I would also like to thank Dr. Demet Uluşen for her beneficial advices and remarks.

Finally, special thanks go to my parents. This work would not have been possible without their endless support.

TABLE OF CONTENTS

LIST OF FIGURES

FIGURES

NOMENCLATURE

Abbreviations

1-D	One-dimensional
2-D	Two-dimensional
CFL	Courant–Friedrichs–Lewy
EP	Electric Propulsion
ESA	European Space Agency
ET	Electric Thruster
GEO	Geostationary Earth Orbit
GRC	Glenn Research Center
HALE	Hall Effect Thruster Development
HET	Hall Effect Thruster
JPL	Jet Propulsion Laboratory
KIAE	Kurchatov Institute of Atomic Energy
MAI	Moscow Aviation Institute
MCC	Monte Carlo Collision
MPDT	MagnetoPlasmaDynamic Thruster
NASA	National Aeronautics and Space Administration
NSTAR	NASA Solar Electric Propulsion Technology Applications Readiness
PIC	Particle-in-Cell
PPT	Pulsed Plasma Thruster
RHS	Right-hand Side
SMART	Small Missions for Advanced Research and Technology
SPT	Stationary Plasma Thruster
TsNIIMASH	Central Research Institute of Machine Building
TAL	Thruster with Anode Layer
TÜBİTAK	The Scientific and Technological Research Council of Turkey
VDF	Velocity Distribution Function

Symbols

B	Magnetic field
D	Diffusion coefficient
D_B	Bohm diffusion coefficient
e	Electron charge
E	Electric field
eV	Energy associated with 1 electron volt
f	Velocity distribution function
g	Gravitational acceleration
I_a	Electron current collected by anode
I_c	Electron current emitted by cathode
I_{cb}	Electron current neutralizing the beam
I_{cp}	Current of primary electrons from the cathode collected by the anode
I_{es}	Current of secondary electrons from the ionization events collected by anode
I_d	Discharge current
I_H	Hall current
I_{sp}	Specific impulse
i	Index of the grid points in position space
j	Current density, index of the grid points in velocity space
J	Discharge current per area in 1-D model
k	Boltzmann's constant
L	Discharge channel length
l_D	Length of the closed drift region
m	Mass, electron mass
$\dot{m}$	Propellant mass flow rate
M	Mass of a xenon atom, spacecraft mass
M_d	Spacecraft dry mass
M_p	Propellant mass
n	Particle density
p	Plasma pressure
P_d	Discharge power
P_{in}	Electric power input

P_{jet}	Jet power
q	Electric charge
r_L	Larmor radius
T	Thrust, temperature in K
T_{eV}	Electron temperature in electron volts
U	Potential
U_b	Beam voltage
U_c	Coupling voltage
U_d	Discharge voltage
U_{ex}	Excitation potential
U_i	Ionization potential
v	Velocity
v_{ex}	Exhaust velocity
v_D	Diamagnetic drift velocity
v_E	$E \times B$ drift velocity
v_{th}	Electron thermal velocity
w	Channel width
Γ	Flux of particles
δ	Dirac delta function
Δv	Change in velocity
η	Resistivity
λ	Mean free path
λ_D	Debye length
μ	Mobility
μ_B	Bohm mobility
ν	Collision frequency
ρ	Charge density
σ_i	Ionization cross-section
σ_{ex}	Excitation cross-section
τ	Collision time
ϕ	Relaxation coefficient
ω	Cyclic frequency
ω_c	Electron cyclotron frequency
ω_p	Electron plasma frequency

Subscripts

a	Neutral atom
e	Electron
f	Final
i	Ion, initial
s	Particle species
$\perp$	Perpendicular
$\parallel$	Parallel
$\wedge$	Transverse

CHAPTER 1

INTRODUCTION

1.1 Motivation

Since the launch of the world's first artificial satellite, the Sputnik 1 in 1957, thousands of spacecrafts have been sent into space. On most of these vehicles, chemical rocket engines have been used for orbit transfer, maneuvring or station keeping purposes. As the performance of these thrusters was constrained by the limited energy contained in the chemical fuel they carry, scientists worked on more efficient ways of propulsion.

Electric propulsion (EP), which encompasses a wide variety of thrusters using electric power to generate thrust, is accepted today as an alternative to chemical propulsion. Since the electric propulsion does not rely on the chemical energy of a fuel but the electric power supplied by an external source, the propellant in electric thrusters (ETs) can be accelerated to very large velocities depending on the electric power available onboard. High exhaust velocities permit ETs to consume less propellant and carry out the tasks unfeasible with chemical thrusters. For the time being, the main drawback of the EP is the low thrust generation due to electric power limitation.

The very first ideas about electric propulsion were proposed at the beginning of the 20th century by Konstantin Tsiolkovsky and Robert Goddard [6]. In later years H. Oberth, V. Glushko and E. Stuhlinger worked on this subject and demonstrated that such propulsion systems could be manufactured and would offer substantial advantages over the chemical rockets [5].

In 1960s, electric thrusters were extensively studied in the USA and the Soviet Union. The leading research centers were the NASA (National Aeronautics and Space Administration), GRC (Glenn Research Center), JPL (Jet Propulsion Laboratory), KIAE (Kurchatov Institute of Atomic Energy) and TsNIIMASH (Central Research Institute of Machine Building) [6, 30]. While the Americans worked mainly on ion thrusters, the Russians focused on Hall effect thrusters (HETs). In 1964, for the first time, an ion engine conceived by Harold R. Kaufman operated in space, on the SERT-1 mission. The first space flight of a HET took place in 1972. A pair of engines, called SPT-50, were installed on the Soviet satellite "Meteor". Since then over 200 HETs have been operated in space.

Until the end of the last century, the primary task of ETs remained as orbit control. The first usage of an ET on a deep space mission was in 1998 when the NASA sent an ion thruster NSTAR to space on Deep Space 1. In 2003, the European Space Agency (ESA) used PPS-1350 HET on the SMART-1 probe which was sent to the moon [6].

Since the invention of EP, the interest in this technology has grown steadily. Today, the tendency is to develop high power high thrust engines for heavy geostationary satellites and for deep space missions. In the long term, very high power electric thrusters (maybe with nuclear power sources) can make the manned interplanetary flight possible .

1.2 Objective

The objective of this thesis is to gain an insight into the fundamental concepts of a Hall effect thruster, to understand the dominating physical processes in its operation, to formulate the operation by relevant physical quantities and finally to predict the thruster performance from these physical quantities. For this purpose, numerical codes have been written based on the physical model proposed by A.I.Morozov, the developer of the first HETs.

At TUBITAK UZAY (Space Technologies Research Institute), a 1.5 kW HET

similar to the standard SPT-100 is being developed in the scope of the HALE (Hall Effect Thruster Development) project. The numerical simulation developed in this thesis will also be applied to the analysis of this new 1.5 kW thruster.

1.3 Thruster Principles

Thrust

Thrust generation in the electric propulsion systems is based on the same principle of thrust generation in the chemical rockets: accelerating mass and ejecting it from the vehicle at high velocity. By the action-reaction law, a force equal and opposite to the time rate of change of the momentum of the ejected material acts on the spacecraft. This propulsive force is called thrust and given by $T = \dot{m}v_{ex}$, where $\dot{m}$ is the mass flow rate of the ejected material and v_{ex} is the exhaust velocity.

Rocket Equation

Thrust accelerates the spacecraft according to Newton's second law. Ignoring drag and gravity losses, the acceleration of the spacecraft can be expressed by

$$M\frac{dv}{dt} = T = \dot{m}v_{ex}. \tag{1.1}$$

where M is the spacecraft total mass and V is the spacecraft velocity. M decreases with time due to the ejected material. Therefore, replacing the mass flow rate $\dot{m}$ in Eq. 1.1 by $-dM/dt$, integration of Eq. 1.1 between initial and final states

$$\int_{v_i}^{v_f} \frac{dv}{v_{ex}} = \int_{M_i}^{M_f} -\frac{dM}{M} \tag{1.2}$$

yields the classical *Rocket Equation* which relates the velocity increment Δv to the exhaust velocity, and to the initial and final mass ratio M_i/M_f.

$$\Delta v = v_{ex} ln \frac{M_i}{M_f}. \tag{1.3}$$

We can rewrite Eq. 1.3 in terms of the required propulsion material ($M_p = M_i - M_f$) to be consumed between initial and final states. Assuming that the final mass is equal to the dry mass of the spacecraft ($M_f = M_d$) (i.e., all the propellant is spent), we obtain

$$M_p = M_d[e^{\Delta v/v_{ex}} - 1]. \tag{1.4}$$

Δv is often used to define the propulsion requirement of a given space mission. Obviously for a given Δv, as the exhaust velocity is higher, the required propellant mass is lower. Therefore, v_{ex} is an important parameter characterizing the performance of a propulsion device . A typical bipropellant rocket engine has $3-4$ km/s exhaust velocity. However, using electric thrusters, exhaust velocities in the range of $10-40$ km/s can be reached [6]. Actually in chemical propulsion, the exhaust velocity is limited by the energy contained in the chemical bonds of the propellant used. Electric thrusters, on the other hand, separate the propellant from the energy source (which is now a power supply) and thus are not subject to the same limitations.

The exhaust velocity superiority of EP makes it suitable for many missions. To illustrate this, consider a geosynchronous satellite which has a dry mass of 1 tonne and which requires $\Delta v = 1.5$ km/s for stationkeeping during its service life of 15 years. If this satellite was propelled by a chemical rocket with a 2 km/s exhaust velocity, it would require 1117 kg of propellant to carry out the mission. On the other hand an electric thruster with a 20 km/s exhaust velocity would accomplish the same mission using only 78 kg of propellant.

Specific Impulse

In propulsion literature, the specific impulse term, I_{sp}, is defined as the ratio of the thrust to the rate of propellant consumption. Specific impulse for constant thrust and propellant flow rate is

$$I_{sp} = \frac{T}{\dot{m}g} = \frac{v_{ex}}{g}, \tag{1.5}$$

where g is the acceleration of gravity, 9.807 m/s. Specific impulse related to the propellant exhaust velocity is a measure of how efficiently thrust is generated.

Total Efficiency

The total efficiency of an electric thruster is defined as the jet power, P_{jet} (kinetic thrust power of the plasma beam leaving the thruster), divided by the total electrical power into the thruster, P_{in}. Expressing the jet power as $\dot{m}v_{ex}^2/2$ and thrust as $T = \dot{m}v_{ex}$ the total efficiency, η_T, can be written as

$$\eta_T = P_{jet}/P_{in} = \frac{T^2}{2\dot{m}P_{in}}. \tag{1.6}$$

Measuring the thruster's input electrical power, propellant mass flow rate, and the thrust generated, the total efficiency of the thruster can be calculated [6].

1.4 Electric Propulsion Types

Electric propulsion be classified in three categories according to the acceleration mechanism of the propellant: electrothermal, electrostatic and electromagnetic.

1.4.1 Electrothermal

In electrothermal thrusters, the propellant heated up by using electric power expands through a nozzle. Transforming the enthalpy of the propellant gas into kinetic energy, thrust is produced. The energy of the gas is determined by its temperature upstream of the nozzle. Resistojets and arcjets are examples of this category. Resistojets use a heating element (ohmic resistor) to raise the temperature of the propellant. Since the heat is transferred to the propellant gas from thruster components, the specific impulse is limited by the maximal temperature attainable by the thruster components, which results in low values such as $300 - 400$ s. The main advantage is the low thrust cost.

To overcome this limitation, arcjets heat the propellant by passing through it a high current arc generated between an upstream conical cathode and a downstream annular anode integral to the exhaust nozzle. In arcjets, the temperature of the gas can significantly surpass the temperature of the electrodes. Consequently the propellant gas is ejected from the nozzle at much higher velocity

compared to resistojets. Depending on the propellant (hydrogen, ammonia or hydrazine) the specific impulse may reach 1000 s. The erosion of the internal cathode, however, is the main drawback in this type of thrusters.

In the early 1980s, resistojets were used for attitude control and station keeping of commercial satellites. The first arcjet was utilized on the satellite AMSAT-OSCAR 13, in 1988 [12]. Figure 1.1 shows the general schematic of the electrothermal thrusters.

1

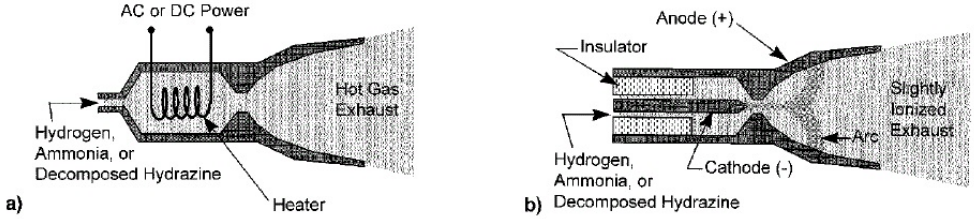

Figure 1.1: a) resistojet, b) arcjet [18]

1.4.2 Electrostatic propulsion

Electrostatic thrusters use electrostatic fields to accelerate a charged propellant. The most common type of electrostatic thrusters is gridded ion engines in which biased grids are used to generate the electric field. In ion thrusters, the propellant gas (usually xenon) is injected in a Kaufmann source, composed of permanent magnets mounted on the surrounding walls. The electrons are supplied by an internal cathode at the base of the Kaufmann source (see Figure 1.2). A voltage is applied between the inner surface of the chamber, acting as an anode, and the internal cathode. The electrons trapped by a magnetic field have enough energy to ionize the injected propellant. At the exit of the Kaufmann source there are two grids. The potential difference between the first grid (positively charged) and the second grid (negatively charged) accelerates the ions. The electrons supplied by an external cathode neutralizes the positively charged propellant to prevent the ions from being attracted back to the

spacecraft (back-streaming ions reduce the net thrust) and to avoid spacecraft charging. Ion thrusters feature very high specific impulse (ranging from 2000 to 10000 s).

The main disadvantage of ion thrusters is the limitation of the ion current density due to the positive charge accumulation between the electrostatic grids. Since electrons are absent in the gap between the grids, the extracted ion current cannot exceed the level at which repulsing ions in the gap would keep new ions from entering. This effect, called the *space charge limitation*, severely reduces the thrust density. Consequently, ion thrusters have a bigger exit area than Hall thrusters for the same thrust.

SERT-1 was the first ion thruster to operate in space (1964). Later in 1998, Deep Space 1 equipped with the NSTAR ion engine became the world's first spacecraft to escape Earth's gravitation from orbit [6] using an electric propulsion system.

1.4.3 Electromagnetic propulsion

Electromagnetic thrusters use both the electric and magnetic fields to accelerate the propellant and produce thrust. Pulsed Plasma thruster (PPT) and Magnetoplasmadynamic thruster (MPDT) belong to this category. In PPTs, a fraction of a solid propellant is ionized by a pulsed discharge. MPDTs (Figure 1.2b) use a very high current to ionize a significant fraction of the propellant. In a MPDT, the propellant injected to the discharge channel is ionized by applying an electric field between the internal cathode and the anode. The current between the anode and the cathode induces a magnetic field perpendicular to the electric field. Therefore, the plasma current experiences the Lorentz force $\mathbf{F} = \mathbf{j} \times \mathbf{B}$, which accelerates the plasma towards the channel exit. When the power supplied to the thruster is low (< 200 kW), the induced magnetic field is too weak to create sufficiently high Lorentz force which will enable plasma acceleration [12]. In practice, an external magnetic field can also be applied in these low power cases. MPDTs provide very high thrust compared to other electric propulsion types but they require very high power for operation. Recently, an MPDT with 12 N thrust, 4500 s specific impulse and 400 kW power was tested

at Princeton University. However, such thrusters are still unpractical for the moment since the solar panels on the conventional platforms cannot meet the high electric power requirement yet. In the future, once the power problem is resolved, manned interplanetary flights can be achieved using MPDTs .

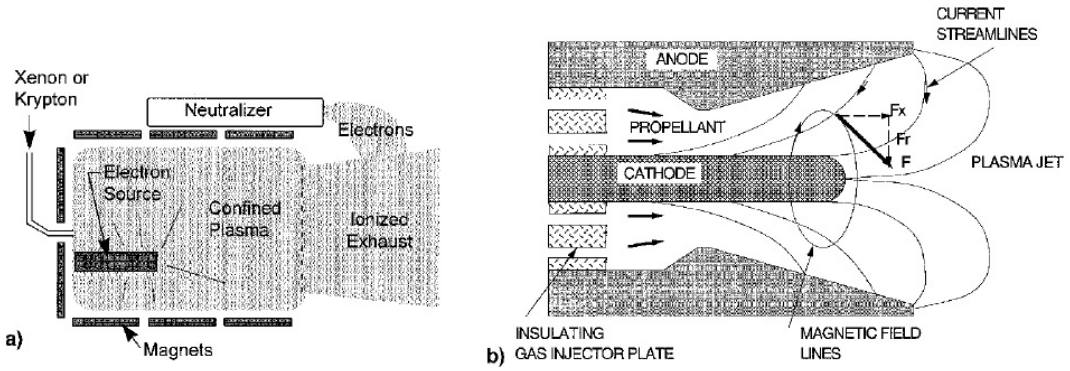

Figure 1.2: a) gridded ion engine, b) MPD thruster [18]

1.5 Hall thrusters

Hall effect thrusters (HET) or Hall thrusters, classified as either electrostatic or electromagnetic thrusters, are the most commonly used type of electric thrusters.

They were developed at the early 1960s in the Soviet Union under the leadership of A.I.Morozov. Researches have been conducted in the institutes including Fakel, TsNIIMASH, MAI and Kurchatov. Since 1960s various Hall thrusters of different sizes and power levels have been elaborated. The first satellite equipped with a Hall thruster (SPT-50) "Meteor" was put into orbit in 1972. Since then HETs have been utilized on the Russian telecommunication satellites series, Gals, Express and Yamal. Among various HETs, SPT-100, which was developed in 1980s, has the most flight heritage. This thruster served as a base model for many other thrusters of smaller or larger sizes.

Soviet-built Hall thrusters were introduced to the West in the early 1990s. Since then, researches on Hall thruster development have also been conducted in the United States, France, Italy and Japan. In 2003, ESA sent to the Moon an

experimental probe, SMART-1, which was propelled by a Hall thruster, PPS-1350, developed by SNECMA in cooperation with Fakel. In 2004, for the first time, a Hall thruster (the Fakel SPT-100) was used by the U.S. on Space Systems Loral's MBSAT. In August 2010 a U.S. military GEO communication satellite equipped with the Aerojet BPT-4000 Hall thrusters was launched into orbit. At 4.5 kW, the BPT-4000 is the most powerful HET which has ever flown in space. This engine with 0.27 N thrust can also provide orbit raising capability besides the orbital station-keeping.

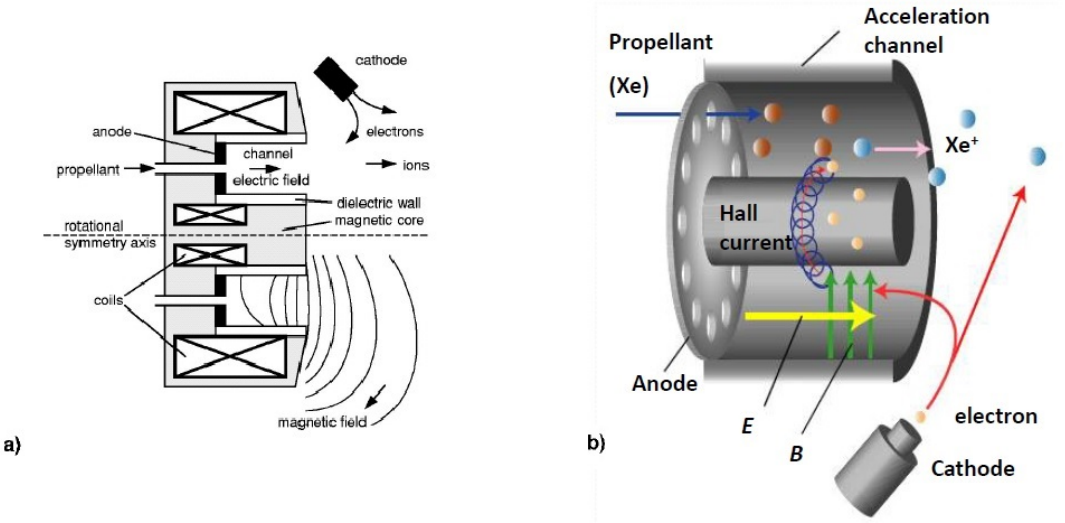

Figure 1.3: a) Hall thruster cross-section [1], b) three dimensional view of a Hall thruster

A Hall thruster has a relatively simple geometry (Figure 1.3a). It consists of an annular discharge channel with an interior anode at its base, and an external cathode near the channel exit. Propellant gas (usually xenon) is injected into the channel from the anode surface. Electrons supplied by the cathode ionize the propellant through collisions. A magnetic circuit creates a radial magnetic field across the channel, which prevents electrons from moving directly to the anode. The electrons with reduced mobility due to the transverse magnetic field spiral along the field lines drifting in the $\mathbf{E} \times \mathbf{B}$ direction and creating azimuthal Hall current as seen in Figure 1.3b. This permits the distribution of the applied discharge voltage along the channel axis and creation of an axial electric field between the anode and the cathode plasma. The ionized propellant

is then accelerated by the electric field and reaches very high exhaust velocities ($\sim$ 16000 m/s) at the channel exit, resulting in the generation of the thrust.

1.6 Outline of the Thesis

The thesis is organized as follows: The second chapter gives an overview of the basic concepts in plasma physics. The third chapter explains the operation principles of a Hall thruster. It also includes a survey of the numerical models that have been developed up to date. The fourth chapter describes the one-dimensional fluid and hybrid models upon which the numerical analysis carried out in this thesis is based. The fifth chapter explains the solution procedure used in the numerical analysis and presents the results from both models. The sixth and final chapter summarizes the thesis findings, and discusses the future work.

CHAPTER 2

BASIC PLASMA PHYSICS

Hall thrusters are devices in which plasma is generated by electrical discharge. Studying Hall thrusters, understanding physical processes in their operation and developing descriptive models require the knowledge of plasma physics. Therefore, in the following sections, the basic concepts of plasma physics are introduced.

2.1 What is a plasma?

The state of a matter is determined by the equilibrium between the random kinetic energy (thermal energy) of the particles that constitute the matter and the binding forces that hold these particles together [2]. By giving heat energy to a solid or liquid, the thermal kinetic energy of the atoms or molecules increases until these particles become able to overcome the binding potential energy. At this point, phase transition occurs and a solid turns into a liquid then into a gas. When a gas is heated up further, its molecules dissociate into atoms as a result of collisions between particles having greater kinetic energy than molecular binding energy. At higher temperatures, some fractions of the atoms possess sufficient kinetic energy to overcome, by collisions, the binding energy of the outermost electrons, and the gas becomes ionized. The ionization increases with temperature and beyond a certain point, the gas becomes a plasma containing many interacting free electrons, ions and neutral particles and having very different properties than an ordinary gas. Due to its distinctive characteristics, plasma is often considered as the fourth state of matter.

The degree of ionization of a gas in thermal equilibrium is given by the Saha equation [8]:

$$\frac{n_i}{n_a} \approx 2.4 \times 10^{21} \frac{T^{3/2}}{n_i} e^{-U_i/kT}. \tag{2.1}$$

Here n_a and n_i denote the number density of neutral and ionized atoms. k is Boltzmann's constant, T and U_i are the gas temperature in K and ionization energy, respectively. The Saha equation tells that any gas is ionized to some degree depending on the temperature. For example, ordinary air at room temperature has $n_i/n_a \approx 10^{-122}$.

As the temperature increases, the gas particles become more energetic. The frequent collisions between them lead to removal of electrons from atoms hence ionization (kT term becomes larger than U_i; and n_i/n_a rises abruptly). Further increase in temperature results in gradual transformation of the ionized gas into plasma state. However, ionization is not the only criterion for defining a plasma since it occurs in any gas to some degree. A plasma is defined as a quasineutral gas of charged and neutral particles exhibiting collective behavior [8].

In an ordinary gas, the motion of a particle is controlled by the collisions it makes with other particles. However, in a plasma, a particle's motion is affected by the electric fields generated by local concentrations of charge and by the magnetic fields induced by the moving charges. Therefore, particles can exert force on each other even at large distances. In some plasmas, these long range forces are much bigger than the forces due to ordinary collisions so that such plasmas are assumed as collisionless. What is meant by the collective behaviour is that long range interactions between the particles.

Quasineutrality and Debye Length

Another property of the plasma is *quasineutrality*. Under equilibrium conditions with no external forces and disturbances, a volume element of plasma, that is sufficiently large to contain a large number of particles and sufficiently small compared to characteristic lengths for the variation of macroscopic parameters such as density and temperature, has no net charge [2]. The reason of this

behavior is that, the microscopic charge concentrations arising in the interior of the plasma cancel each other and result in zero net charge on a macroscopic scale. If the macroscopic neutrality was not maintained, the resulting coulomb forces between space charge fields would be enormous compared to the particle thermal kinetic energy.

In a plasma, the thermal particle energy tends to disturb the electrical neutrality, on the other hand the electrostatic potential energy tends to restore it. In the absence of external disturbances, excess space charges can occur only over distances in which the thermal particle energy balances the electrostatic potential energy resulting from any charge separation. This distance is on the order of a characteristic length parameter of the plasma, the *Debye length* (λ_D), which is defined as

$$\lambda_D = \left(\frac{\epsilon_0 kT}{n_e e^2} \right)^{1/2}, \tag{2.2}$$

where e is the electron charge, n_e is the electron density and ϵ_0 is the permittivity of free space. In the absence of external forces, the plasma cannot allow violation of macroscopic neutrality over distances larger than λ_D. Because, the electric field, arising from the charge accumulation, redistributes the charges so that the regions of excess charge are neutralized.

Associated with the "quasineutrality" property, another fundamental characteristic of a plasma is its ability to shield out electric potentials that are applied to it. When a test charge q is inserted into a plasma, it is observed that a cloud of particles of opposite charge simultaneously surrounds it. As a result of this charge accumulation, the potential falls quickly in the vicinity of the test charge. Therefore, the potential difference between the plasma and the inserted charge is not distributed throughout the bulk plasma but in a very thin layer. The thickness of this layer is on the order of Debye length and it is called *plasma sheath*. In this thin layer, charge neutrality does not hold. However, the bulk of the plasma maintains its quasineutrality.

An ionized gas can be considered as a plasma if its density is high enough such

that Debye length, λ_D, is much smaller than the characteristic dimension of the plasma system, L (i.e., $\lambda_D << L$). This criterion ensures that in plasmas, local charge concentrations are allowed only in a small distance compared with L, leaving the bulk of the plasma free of large electric potentials. Also, this condition is valid only if there are enough particles in the charge cloud: The number of particles in a Debye sphere, N_D, must be much greater than 1 (i.e., $N_D = 4n\pi\lambda_D^3/3 >> 1$).

Plasma frequency

When a plasma is instantaneously disturbed from the equilibrium conditions by an external force (for example, electrons are displaced from a uniform background of ions), electric field resulting from charge separation accelerates the electrons in such a direction to restore the neutrality of the plasma. Electrons having much smaller mass will oscillate around the heavier ions until they return back to their equilibrium positions. These oscillations of electrons are characterized by a natural frequency, called the *(electron) plasma frequency*, ω_p, given by

$$\omega_p = \left(\frac{n_e e^2}{m_e \epsilon_0}\right)^{1/2}, \tag{2.3}$$

where m_e is the electron mass. Collisions between electrons and neutral particles tend to damp these oscillations by dissipative mechanisms. If the electron neutral collision frequency, ν_{en}, is higher than the plasma frequency, electrons will be forced by these collisions to be in equilibrium with neutrals, in which case the medium can be treated as a neutral gas. Therefore, another condition of plasmas is $\omega_p\tau > 1$, where $\tau = 1/\nu_{en}$ denotes the average time between electron-neutral collisions. It implies that in a plasma this average time must be large compared to the characteristic time during which the plasma parameters are changing. In a weakly ionized gas, the charged particles collide so frequently with neutral atoms that their motion is controlled by ordinary aerodynamic forces rather than by electromagnetic forces. However, in plasmas, the situation is the opposite.

To summarize, a plasma must satisfy the following three conditions:

1. $\lambda_D << L$

2. $N_D >>> 1$

3. $\omega_p \tau > 1$

2.2 Maxwell's Equations

In electric propulsion devices, electromagnetic fields obey *Maxwell's equations* formulated in a vacuum that contains charges and currents:

$$\nabla \cdot \mathbf{E} = \frac{\rho}{\epsilon_0}, \quad \nabla \times \mathbf{E} = -\frac{\partial \mathbf{B}}{\partial t}, \quad \nabla \cdot \mathbf{B} = 0, \quad \nabla \times \mathbf{B} = \mu_0 \left(\mathbf{j} + \epsilon_0 \frac{\partial \mathbf{E}}{\partial t} \right). \quad (2.4)$$

where ρ, $\mathbf{j}$, ϵ_0, μ_0 denote, respectively, the total charge density, the total electric current density, the electric permittivity, and the magnetic permeability of free space. In ρ and $\mathbf{j}$ terms, all the charges and currents for all the plasma species, as well as multiply charged ions are included. They can be expressed, respectively as

$$\rho = \sum_s q_s n_s = e(Z n_i - n_e), \quad \mathbf{j} = \sum_s q_s n_s \mathbf{v}_s = e(Z n_i \mathbf{v}_i - n_e \mathbf{v}_e) \quad (2.5)$$

where q_s is the charge and v_s is the velocity of the charge species s and subscripts i and e correspond to ions and electrons, respectively. Z denotes the the charge state.

In the case of static magnetic field ($\partial \mathbf{B}/\partial t = 0$), the curl of the electric field becomes zero hence it can be expressed as the gradient of the electric potential, U,

$$\mathbf{E} = -\nabla U. \quad (2.6)$$

Substituting $\mathbf{E}$ in the first of the Maxwell equations (2.4), the Poisson equation is obtained:

$$\nabla^2 U = -\frac{\rho}{\epsilon_0}. \quad (2.7)$$

2.3 Single particle motion

A plasma contains charged particles which are subject to electromagnetic forces. The motion of a single charged particle in the presence of electric and magnetic fields is described by the Lorentz force equation:

$$m\frac{d\mathbf{v}}{dt} = q(\mathbf{E} + \mathbf{v} \times \mathbf{B}). \tag{2.8}$$

In the case $\mathbf{E} = 0$, taking $\mathbf{z}$ to be the direction of $\mathbf{B}$ ($\mathbf{B} = B\mathbf{z}$), we have

$$m\dot{v}_x = qBv_y, \qquad m\dot{v}_y = -qBv_x, \qquad m\dot{v}_z = 0. \tag{2.9}$$

Taking derivatives of both sides in the first two of the above equations, we get $\ddot{v}_x$

$$\ddot{v}_x = \frac{qB}{m}\dot{v}_y = -\left(\frac{qB}{m}\right)^2 v_x, \qquad \ddot{v}_y = -\frac{qB}{m}\dot{v}_x = -\left(\frac{qB}{m}\right)^2 v_y. \tag{2.10}$$

These equations describe a simple harmonic oscillator at the *cyclotron frequency*:

$$\omega_c = \frac{|q|B}{m}. \tag{2.11}$$

The solution to Eq. 2.10 is

$$v_{x,y} = v_\perp exp(\pm i\omega_c t), \tag{2.12}$$

where $v_\perp$ is a positive constant speed in the plane perpendicular to $\mathbf{B}$. Taking time integrals of the velocities found in Eq. 2.12 and taking real parts of Eq. 2.12, particle position is obtained as a function of time

$$x - x_0 = r_L sin(\omega_c t), \qquad y - y_0 = \pm r_L cos(\omega_c t) \tag{2.13}$$

where r_L is the *Larmor radius* which is given by

$$r_L = \frac{v_\perp}{\omega_c} = \frac{m v_\perp}{|q|B}. \tag{2.14}$$

These results mean that a charged particle with a velocity, $v_\perp$, in the presence of a magnetic field makes a circular motion with the radius r_L, in a plane perpendicular to the magnetic field about a guiding center (x_0, y_0). In addition, if the particle has a velocity v_z, along the magnetic field, as its motion in the parallel direction is not affected by $\mathbf{B}$, its trajectory forms a helix. Obviously electrons having the same velocity with the ions have smaller r_L and larger ω_c due to their lower mass.

Now, assume that in addition to $\mathbf{B}$, an electric field also exists and lies in the $x - z$ plane so that $E_y = 0$. The equations of motion, then, become:

$$\dot{v}_z = \frac{q}{m} E_z, \qquad \dot{v}_x = \frac{q}{m} E_x \pm \omega_c v_y, \qquad \dot{v}_y = \mp \omega_c v_x. \tag{2.15}$$

The solution of Eq. 2.15 is

$$v_z = \frac{q E_z}{m} t + v_{z0}, \qquad v_x = v_\perp e^{i\omega_c t}, \qquad v_y = \pm i v_\perp e^{i\omega_c t} - E_x/B. \tag{2.16}$$

In this case, the Larmor motion is the same as before, but now the guiding center is drifting with a constant velocity of $v_E = E_x/B$ in the $-y$ direction (for $E_x > 0$).

A general formula for the drift velocity can be obtained by solving Eq. 2.8 in vector form. Considering the drift to be steady state, the term $m d\mathbf{v}/dt$ in Eq. 2.8 can be omitted [6]. Then the drift velocity is found as

$$\mathbf{v}_E = \frac{\mathbf{E} \times \mathbf{B}}{B^2}, \tag{2.17}$$

pointing in the direction perpendicular to both electric and magnetic fields.

2.4 Kinetic Theory

A plasma system contains a vary large number of interacting charged particles. As it is not practical to track all these individual particles, a statistical ap-

proach is more convenient. In kinetic theory, plasma species are represented by a velocity distribution function, $f(\mathbf{r}, \mathbf{v}, t)$ defined in position and velocity spaces.

The f function gives the probable number of particles to be found in a unit volume, at position $\mathbf{r}$ and time t, having velocity components between v_x and $v_x + dv_x$, v_y and $v_y + dv_y$ and v_z and $v_z + dv_z$ The integration of f over the velocity space gives the particle number density at a position and time, $n(\mathbf{r}, t)$.

$$n(\mathbf{r}, t) = \int_{-\infty}^{\infty} f(\mathbf{r}, \mathbf{v}, t) d\mathbf{v} \tag{2.18}$$

Here $d\mathbf{v}$ denotes an infinitesimal volume element $dv_x dv_y dv_z$ in velocity space. For convenience, a normalized velocity distribution function is defined, $\hat{f}(\mathbf{r}, \mathbf{v}, t) = f(\mathbf{r}, \mathbf{v}, t)/n(\mathbf{r}, t)$ such that the following integral gives unity,

$$\int_{-\infty}^{\infty} \hat{f}(\mathbf{r}, \mathbf{v}, t) d\mathbf{v} = 1. \tag{2.19}$$

Hence, $\hat{f}(\mathbf{r}, \mathbf{v}, t) d\mathbf{v}$ gives the probability that a particle, at a given position and time, has velocity components between $\mathbf{v}$ and $\mathbf{v} + d\mathbf{v}$.

The macroscopic variables such as flow velocity, kinetic pressure, thermal energy flux can be considered as average values of physical quantities involving the collective behavior of a large number of particles. Therefore, these variables can be calculated by taking various moments of the distribution function in the following way:

$$\langle Q(\mathbf{r}, \mathbf{v}, t) \rangle = \frac{1}{n(\mathbf{r}, t)} \int_{-\infty}^{\infty} Q(\mathbf{r}, \mathbf{v}, t) f(\mathbf{r}, \mathbf{v}, t) d\mathbf{v} = \int_{-\infty}^{\infty} Q(\mathbf{r}, \mathbf{v}, t) \hat{f}(\mathbf{r}, \mathbf{v}, t) d\mathbf{v}. \tag{2.20}$$

Here $Q(\mathbf{r}, \mathbf{v}, t)$ is some particle property (It may be the mass, velocity, momentum, or energy of the particle) and $\langle Q(\mathbf{r}, \mathbf{v}, t) \rangle$ stands for the average value of this property with respect to velocity space. The average value is a macroscopic quantity always independent of $\mathbf{v}$, being a function of only $\mathbf{r}$ and t.

The fundamental differential kinetic equation which the distribution function

has to satisfy is the *Boltzmann equation*:

$$\frac{\partial f_s}{\partial t} + \mathbf{v} \cdot \nabla f_s + \frac{\mathbf{F}}{m_s} \cdot \nabla_v f_s = \left(\frac{\delta f_s}{\delta t}\right)_{coll} \tag{2.21}$$

where f_s is the velocity distribution function for the species, s, the right hand side (RHS) term represents the rate of change of f_s (the net loss or gain of s type particles due to collisions) and $\mathbf{F}$ is the force acting on the particles. For a collisionless plasma the RHS is zero and if the force $\mathbf{F}$ is entirely electromagnetic (Lorentz force in Eq. 2.8) the *Boltzmann equation* takes the special form

$$\frac{\partial f_s}{\partial t} + \mathbf{v} \cdot \nabla f_s + \frac{q_s(\mathbf{E} + \mathbf{v} \times \mathbf{B})}{m_s} \nabla_v f_s = 0 \tag{2.22}$$

which is called the *Vlasov equation*. Here q_s is the charge of a particle of type s.

The equilibrium distribution function is the time independent ($\partial f/\partial t = 0$) solution of the Boltzmann equation in the absence of external forces ($F_{ext} = 0$). In the equilibrium state the particle interactions do not cause any change in the distribution function with time and there are no spatial gradients in the particle number density. Under these conditions, the distribution function is homogeneous ($\nabla f = 0$ and $f = f(v)$). The velocity distribution function satisfying the Boltzmann equation with the conditions mentioned above and therefore representing the equilibrium state is called *Maxwell-Boltzmann* or *Maxwellian* distribution function and it has the form

$$\hat{f}(\mathbf{v}) = \left(\frac{m}{2\pi kT}\right)^{1/2} exp\left(-\frac{m\mathbf{v}^2}{2kT}\right). \tag{2.23}$$

The average kinetic energy of a particle in the Maxwellian distribution in three dimensions is

$$E_{ave} = \langle \frac{1}{2} m\mathbf{v}^2 \rangle = \int_{-\infty}^{\infty} \frac{1}{2} m\mathbf{v}^2 \hat{f}(\mathbf{v}) d\mathbf{v} = \frac{3}{2} kT. \tag{2.24}$$

Since T is related to average energies of particles, it is very common in plasma physics to give temperatures in units of energy such as eV(electronvolt). For $kT = 1\ eV = 1.6 \times 10^{19}\ J$, we have $T = \frac{1.6 \times 10^{-19} J}{1.38 \times 10^{-23} J/K} = 11600\ K$. Thus the

conversion factor is $1\ eV = 11600\ K$. For example, a 10 eV plasma means that $kT = 10\ eV$ and $T = 1,16 \times 10^5\ K$.

The velocity distribution functions hence the energies of the particles tend to equilibrate via collisions between like particles and between different species. It often happens in a plasma that the ions and the electrons have separate Maxwellian distributions with different temperatures, T_i and T_e. The reason of this is that the collision rate among ions or among electrons themselves is larger than the rate of collisions between an ion and an electron. Each species reach its own thermal equilibrium long before the equalization of the two temperatures. Actually the plasma may not last so long that the temperature equalization of different species occurs. This is why a plasma is generally characterized by separate temperatures for electrons and ions.

2.5 Transport Equations

In the previous section, it has been mentioned that macroscopic variables can be obtained from the velocity distribution function. However, instead of solving the Boltzmann equation for the distribution function, the differential equations governing the macroscopic variables can be derived directly from the Boltzmann equation by taking its moments. Multiplying the Boltzmann equation by $1, \mathbf{v}$ and $v^2/2$, respectively and integrating over the velocity space give the three *macroscopic transport equations*: conservation of particles, momentum and energy.

In many cases, the plasma species are treated as fluids assuming that they have Maxwellian velocity distributions. In this case they are described by the following fluid equations.

2.5.1 Particle Conservation

The continuity equation describes the conservation of particles and/or charges in the plasma and it is given by

$$\frac{\partial n_s}{\partial t} + \nabla \cdot (n_s \mathbf{v}_s) = \dot{n}_s, \tag{2.25}$$

where $\dot{n}_s$ represents a source or sink term for a plasma species, s.

2.5.2 Momentum Conservation

The momentum transfer for each particle species s is described by the following equation:

$$\begin{aligned} m_s n_s \frac{d\mathbf{v}_s}{dt} &= m_s n_s \left[\frac{\partial \mathbf{v}_s}{\partial t} + (\mathbf{v}_s \cdot \nabla)\mathbf{v}_s \right] \\ &= q_s n_s (\mathbf{E} + \mathbf{v}_s \times \mathbf{B}) - \nabla \cdot \mathbf{p}_s - m_s n_s \sum_{s,r} \nu_{sr}(\mathbf{v}_s - \mathbf{v}_r). \end{aligned} \tag{2.26}$$

The forces represented on the right-hand side of Eq. 2.26 are the Lorentz force, the pressure gradient ($\mathbf{p}_s$) force and the forces due to collisions, respectively. If the pressure is isotropic, it is a scalar given by $P = nkT$. In the collision term, ν_{sr} is the collision frequency between species s and r.

2.5.3 Energy Conservation

For a charged species s, moving with velocity v_s, the energy equation is given in a general form by

$$\begin{aligned} \frac{\partial}{\partial t}\left(n_s m_s \frac{{v_s}^2}{2} + \frac{3}{2} p_s \right) + \nabla \cdot \left(n_s m_s \frac{{v_s}^2}{2} + \frac{5}{2} p_s \right) \mathbf{v}_s - \nabla \cdot (K_s \nabla T_s) \\ = q_s n_s \left(\mathbf{E} + \frac{\mathbf{R}_s}{q_s n_s} \right) \cdot \mathbf{v}_s + Q_s - \Psi_s. \end{aligned} \tag{2.27}$$

On the left-hand side, the first divergence term represents the macroscopic energy flux, the second the work done by the pressure and the third the heat conduction. K_s denotes the thermal conductivity.

The first term on the right-hand side of Eq. 2.27 is the Joule heating. The term, R_s, represents the momentum change of particles s as a result of collisions with

other particles. Q_s represents the heat generated/lost due to elastic collisions and Ψ_s, is the energy loss due to inelastic collision processes such as excitation and ionization.

2.6 Collisions and Ionization

As already expressed in previous sections, charged particles in a plasma undergo collisions with other charged particles and neutral atoms which allow momentum transfer between them. Many plasma processes and properties such as ionization rate, diffusion, mobility, and resistivity depend on the collision rate of the particles. Collision frequencies strongly depend on the particle velocities and collision cross-sections. To illustrate this, consider a thin slice with an area, A, and a thickness, dx, containing neutral gas atoms which are spheres of cross-sectional area, σ. The number of atoms in the slice is $n_a A dx$, where n_a is the density of the neutral gas. Assume that fast-moving charged particles are incident upon the slice(Fig. 2.1).

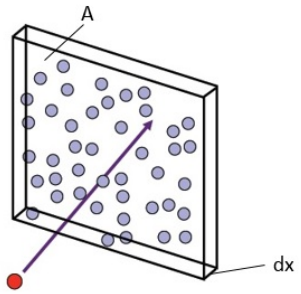

Figure 2.1: a slice of neutral gas with an area of A and a thickness of dx (taken from)

The spheres occupy a fraction of the slice area, $n_a A\sigma dx/A = n_a \sigma dx$. If the incident flux of particles is Γ, then the flux that emerges on the other side of the slice without making a collision is

$$\Gamma' = \Gamma(1 - n_a \sigma dx). \tag{2.28}$$

The change in the flux as the particles pass through the slice can be written as

$$d\Gamma/dx = -\Gamma n_a \sigma. \tag{2.29}$$

The solution to Eq. 2.29 is

$$\Gamma = \Gamma_0 e^{-n_a \sigma x} = \Gamma_0 e^{-x/\lambda}. \tag{2.30}$$

In a distance λ, the particle flux would decrease to $1/e$ of its initial value. This quantity, λ, is the *mean free path* for particle collisions:

$$\lambda = \frac{1}{n_a \sigma}. \tag{2.31}$$

Therefore, the mean time between collisions can be calculated by the mean free path divided by the charged particle velocity v:

$$\tau = \frac{\lambda}{v} = \frac{1}{n_a \sigma v}. \tag{2.32}$$

The mean frequency of collisions is then $\tau^{-1} = v/\lambda$. Averaging over particles of all velocities v in a Maxwellian distribution, the collision frequency can be expressed as $\nu = n_a \langle \sigma v \rangle$.

In the case of a relatively slowly moving particle, such as a neutral atom incident on a volume containing fast-moving electrons, the mean free path for the neutral atom is given by

$$\lambda = \frac{v_a}{n_e \langle \sigma v_e \rangle}, \tag{2.33}$$

where v_a and v_e are the neutral atom and the electron velocities respectively.

The neutral atoms are ionized as a result of the inelastic electron-neutral collisions. The ionization rate coefficient is $\langle \sigma_i v_e \rangle$, which is the ionization cross section, σ_i, averaged over the electron velocity distribution function. The ionization rate coefficient for a Maxwellian electron velocity distribution is given in Appendix A. The ion production rate per unit volume is given as a function of this coefficient and neutral and electron densities:

$$\frac{dn_i}{dt} = n_a n_e \langle \sigma_i v_e \rangle. \tag{2.34}$$

The inelastic electron-neutral collisions may also result in the excitation of the neutral atoms. The production rate per unit volume of excited neutrals, n_{ex}, is

$$\frac{dn_{ex}}{dt} = \sum_j n_a n_e \langle \sigma_{ex} v_e \rangle_j, \tag{2.35}$$

where σ_{ex} is the excitation cross section. The excitation rate coefficient is averaged over the electron distribution function and summed over all possible excited states j.

2.7 Diffusion and Mobility

In a plasma, particles tend to diffuse to lower density regions. The simplest case of diffusion is observed under zero magnetic field and an expression for the diffusion can be found from the fluid equation of motion:

$$mn\frac{d\mathbf{v}}{dt} = qn\mathbf{E} - \nabla \cdot \mathbf{p} - mn\nu(\mathbf{v} - \mathbf{v}_0). \tag{2.36}$$

In this case, further assume that the velocity of the particle species of interest is large compared to the other species($\mathbf{v} >> \mathbf{v}_0$) and the plasma is isothermal, $\nabla p = kT\nabla n$. Also let the diffusion be steady state and assume that it is occurring with a sufficiently high velocity such that the convective derivative can be neglected. Eq. 2.36 can then be solved for the particle velocity:

$$\mathbf{v} = \frac{q}{m\nu}\mathbf{E} - \frac{kT}{m\nu}\frac{\nabla n}{n}. \tag{2.37}$$

In Eq. 2.37 the coefficient in front of the electric field is called the *mobility*:

$$\mu = \frac{|q|}{m\nu}. \tag{2.38}$$

Similarly, the coefficient of the density gradient term is called the *diffusion coefficient*:

$$D = \frac{kT}{m\nu}. \tag{2.39}$$

Therefore the mobility is related to the diffusion coefficient as in the following equation, known as *Einstein relation*:

$$\mu = \frac{|q|D}{kT}. \tag{2.40}$$

In the presence of a magnetic field, charged particle motion can be analyzed in two separate directions. Along the magnetic field lines, mobility and diffusion have the same expressions as in the $B = 0$ case (Eq. 2.38 and Eq. 2.39), since $\mathbf{B}$ does not affect the motion of the particles in parallel direction. However, in the perpendicular direction, the magnetic field strength influences the mobility and diffusion coefficients. Therefore, by applying a magnetic field, the plasma diffusion can be reduced as in the case of electron confinement in Hall thrusters.

The perpendicular component of the fluid equation of motion for either species with the same assumptions used in the magnetic field-free case is written as follows

$$mn\frac{d\mathbf{v}_\perp}{dt} = qn(\mathbf{E} + \mathbf{v}_\perp \times \mathbf{B}) - kT\nabla n - mn\nu\mathbf{v}_\perp = 0. \tag{2.41}$$

With $\mathbf{B} = B(z)$, the x and y components of the above equation in (x, y, z) rectangular coordinate system are

$$mn\nu v_x = qnE_x - kT\frac{\partial n}{\partial x} + qnv_yB, \qquad mn\nu v_y = qnE_y - kT\frac{\partial n}{\partial y} + qnv_xB. \tag{2.42}$$

Using the definitions of μ, D and ω_c, the x and y components of the velocity can be written as

$$v_x = \mu E_x - kT\frac{\partial n}{\partial x} + qnv_yB, \qquad v_y = \mu E_y - kT\frac{\partial n}{\partial y} + qnv_xB. \tag{2.43}$$

Solving these two equations, v_x and v_y are found. Then the perpendicular velocity can be written in vector form as

$$\mathbf{v}_\perp = \pm\mu_\perp\mathbf{E} - D_\perp\frac{\nabla n}{n} + \frac{\mathbf{v}_E + \mathbf{v}_D}{1 + (\nu^2/{\omega_c}^2)}. \tag{2.44}$$

Here, $\mu_\perp$ is the perpendicular electron mobility,

$$\mu_\perp = \frac{\mu}{1 + {\omega_c}^2/\nu^2}, \tag{2.45}$$

$D_\perp$ is the perpendicular diffusion coefficient,

$$D_\perp = \frac{D}{1 + {\omega_c}^2/\nu^2}, \tag{2.46}$$

$\mathbf{v}_E$ is the $\mathbf{E} \times \mathbf{B}$ drift (Eq. 2.17) and $\mathbf{v}_D$ is the the diamagnetic drift,

$$\mathbf{v}_D = -\frac{kT}{qB^2}\frac{\nabla n \times \mathbf{B}}{n}. \tag{2.47}$$

From Eq. 2.44, it is evident that drifts are slowed down by collisions with neutrals; the drag factor is $1 + \nu^2/{\omega_c}^2$. The mobility and diffusion drifts, compared to the $\mathbf{B} = 0$ case, are reduced by the factor $1 + {\omega_c}^2/\nu^2$. When ${\omega_c}^2/\nu^2 << 1$, the magnetic field has little effect on diffusion. When ${\omega_c}^2/\nu^2 >> 1$, however, the magnetic field significantly retards the rate of diffusion across $\mathbf{B}$. In this case,

$$D_\perp = \frac{kT}{m\nu}\frac{1}{{\omega_c}^2/\nu^2} = \frac{kT\nu}{m{\omega_c}^2}. \tag{2.48}$$

Contrary to $\mathbf{B} = 0$ case, where diffusion is inhibited by collisions (in Eq. 2.39, ν is on the denominator), in the $B \neq 0$ case, collisions enhance the cross-field diffusion (in Eq. 2.48, ν is on the numerator). That means, without collisions, particles are totally confined by the magnetic field and they do not diffuse at all.

The classical cross-field diffusion coefficient derived above is proportional to $1/B^2$. However, in the laboratory experiments of many devices, including Hall thrusters, the perpendicular diffusion coefficient over some regions is found to be close to the following expression, which is called the *anomalous Bohm diffusion coefficient* [6]:

$$D_B = \frac{kT_e}{16eB}. \tag{2.49}$$

Collisions of electrons with other species lead to resistivity which causes the so called *ohmic heating*. The momentum equation (Eq. 2.26) for electrons, assuming steady state and neglecting electron inertia, can be written as

$$0 = -en(\mathbf{E} + \mathbf{v}_e \times \mathbf{B}) - \nabla \cdot \mathbf{p}_e - mn[\nu_{ei}(\mathbf{v}_e - \mathbf{v}_i) + \nu_{en}(\mathbf{v}_e - \mathbf{v}_a)]. \tag{2.50}$$

Here, both electron-ion and electron-neutral collisions are taken into account. Neglecting v_a (since it is typically very small with respect to electron velocity) and using the charged particle current density given by $\mathbf{j} = qnv$, the above equation can be rewritten as

$$\eta \mathbf{j}_e = \mathbf{E} + \frac{\nabla \cdot \mathbf{p}_e - \mathbf{j}_e \times \mathbf{B}}{en} - \eta_{ei} \mathbf{j}_i. \tag{2.51}$$

This is the *Ohm's law* for partially ionized plasmas. Here, η is the total resistivity and defined as

$$\eta = \frac{m(\nu_{ei} + \nu_{en})}{e^2 n}. \tag{2.52}$$

η_{ei} is the plasma resistivity due to only electron-ion collisions:

$$\eta_{ei} = \frac{m\nu_{ei}}{e^2 n}. \tag{2.53}$$

The resistivity term is related to mobility such that $\eta = 1/(en\mu)$. Also note that the conductivity, σ, is the inverse of the resistivity, $\sigma = 1/\eta$.

CHAPTER 3

THEORY OF HALL THRUSTERS

The main components of a Hall thruster and its operation principles have been explained briefly in Section 1.4. Here, the physics of the Hall thrusters will be analyzed in more detail.

3.1 General properties of a Hall Thruster

In Hall thrusters, a potential difference, U_d, generated by the discharge power supply is applied between the anode and the cathode. From the anode, the neutral propellant gas is injected into the discharge channel (Figure 1.3). The cathode, located outside the channel, ejects electrons, some fraction of which ($\sim 1/3$) ionizes the propellant gas through collisions with neutral atoms. The rest of the electrons neutralizes the ion beam leaving the discharge channel.

A magnetic circuit generates an axisymmetric magnetic field primarily in the radial direction between the inner and outer poles. The magnetic circuit consists of inner and outer coils which are most typically connected in series to the power supply. By using the magnetic field, the mobility of the electrons flowing from the cathode to the anode is reduced (see Sec. 2.7). These electrons spiral along the the magnetic field lines with a Larmor radius (Eq. 2.14) and drift in the $\mathbf{E} \times \mathbf{B}$ direction. Since the motion of electrons across the magnetic field lines is slowed down, their travel time to the anode is significantly increased. This elongated travel time of electrons in the channel permits first of all to efficiently ionize the propellant and secondly to distribute the applied discharge voltage

along the channel axis in such a way that the created axial electric accelerates the ions. However, the electrons are not permanently confined: they diffuse by collisional processes toward the anode and channel walls. Electrons, reaching the anode, pass through the outer circuit and are then emitted from the cathode to complete the circuit.

3.2 Types of Hall Thrusters

There are two main variants of Hall thrusters depending on the material of the discharge channel. The thrusters having dielectric insulating channel walls are called *stationary plasma thruster* (SPT). The walls are manufactured from ceramics such as boron nitride (BN), borosil ($BN - SiO_2$) or alumina (Al_2O_3). The second version of Hall thrusters, having metallic conducting walls are called *thruster with anode layer* (TAL). Although the basic operation principles mentioned in the previous section are the same for both types, they have some distinctive features.

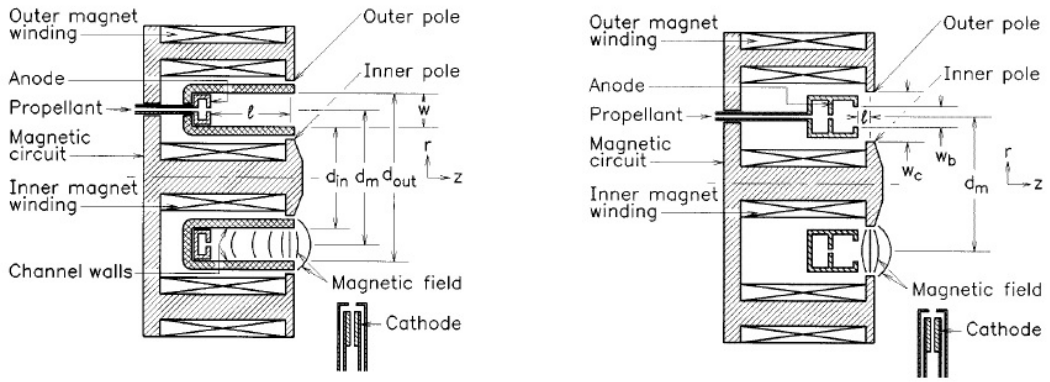

Figure 3.1: schematic of SPT (left) and TAL (right) type Hall Thrusters [31].

In SPTs, the ceramic wall is critical in the discharge. The collisions of charged particles with the walls generate low energy secondary electrons which lower the electron temperature in the discharge plasma. As a result of the low electron temperature, the acceleration process is more extended and gradual. The channel length of this type of thrusters, L, is greater then the channel width, w (in

general $L \approx 2w$).

In TALs, without the reduction of the electron temperature, the plasma potential increases sharply toward the anode such that the ion generation and acceleration occur mainly in a very thin layer near the anode. Therefore ionization and acceleration region is shorter in this type of thrusters. The channel length in TALs is smaller than the channel width. The channel wall is biased negatively such that it repels the electrons. Consequently, the electron impingement on the walls and electron-power losses are reduced. The schematic of both types of Hall thrusters are shown in Fig. 3.1.

Until now only SPTs had flight experience except one TAL model, D-55. In this thesis, the SPT type is the subject of the study.

3.3 Propellant

The most common propellant used in Hall thrusters is xenon. As an inert gas, it does not react with the spacecraft therefore the spacecraft contamination is minimized. Moreover, compared with the other inert gases (argon, krypton and neon), Xenon has a higher atomic weight but a moderate ionization energy. Therefore, it has the lowest ratio of ionization energy to propellant mass. This advantage makes a Hall thruster work more efficiently on xenon than the other inert gases at similar discharge voltages. The disadvantage of the xenon is its high cost and low availability. Therefore, some inert gases have been studied as an alternative to xenon and tested in laboratory experiments. In missions with high specific impulse requirement, the relatively higher ionization energy per unit mass may not cause a serious problem and therefore other inert gases may be utilized [31].

3.4 Magnetic and Electric Fields

The axial variation of the radial magnetic field magnitude in Hall thrusters has the typical distribution shown in Fig. 3.2, having a maximum near the

channel exit and decreasing toward the anode [6]. In the strong magnetic field region, the electrons have reduced mobility and they experience heating due to collisions. The high electron temperature in this region provides high ionization rate. Consequently, the axial electric field also reaches its maximum near the channel exit plane (Fig. 3.2). The region located upstream of the electric field peak is called the "ionization region". Here, almost all neutral atoms are ionized before leaving the channel through collisions with the energetic electrons. The ionization rate coefficient ($\langle \sigma_i v_e \rangle$ in Eq. 2.34) is a function of the electron velocity and ionization cross-section, both of which depend on the electron temperature. For Maxwellian electrons, $\langle \sigma_i v_e \rangle$ is given in Appendix A.

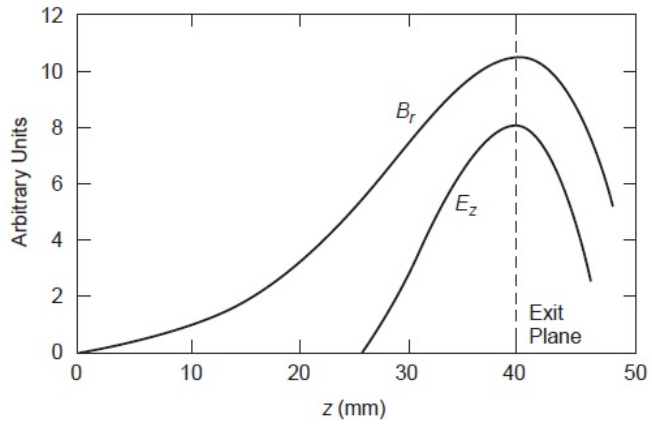

Figure 3.2: Typical radial magnetic field and axial electric field profiles in a HET [6].

Ions in the discharge channel are mostly singly charged. The reason of this is that once the ions are created they are quickly accelerated by the electric field and ejected from the channel before another collision with an electron takes place and one more electron is removed from the ion. However, multiply charged ions also exist in the channel. Such ions are produced in general as a result of single collisions with electrons that have sufficient energy to remove more than one electron in a single collision from a neutral atom. The energy required for such collisions is high and the cross sections for multiple ionization in a single collision are small. As a consequence, the amount of multiply charged ions is relatively small (10-15 % of the ions [23]).

The region near the exit plane where the electric field peaks is called the *acceleration region*. Since the ions may be generated at any location throughout the channel of the thruster, there is no a distinct boundary between the ionization and acceleration regions [31].

The velocity that an ion reaches at the end of the acceleration region depends on the potential at the location where it is generated. Therefore, the maximum velocity of a singly charged ion at the channel exit is

$$v_{max} = \left(\frac{2e}{M}(U_d - \Delta)\right)^{1/2}, \tag{3.1}$$

where Δ is the voltage spent for ionization. At $\Delta = 0$ and for $U_d = 300$ V v_{max} is found approximately as 21 km/s for Xe^+. Experimentally, the mean ion energy corresponds to $70 - 90$ % of U_d.

In the region where the magnetic field is large, the electrons confined by the $\mathbf{B}$ drift in the $\mathbf{E} \times \mathbf{B}$ direction, which is normal to the electric and magnetic fields. As the $\mathbf{B}$ is almost radial (B_r) and $\mathbf{E}$ is almost axial (E_z), the electrons drift in the azimuthal direction ($\hat{\theta}$ in cylindrical coordinates). This strong magnetic field region which spans the ionization and the acceleration regions is often called the closed drift region and it covers a significant fraction of the total channel length.

The closed drift region has an annular shape. The radial width (the difference between the outer and inner radii), w, is much smaller than the channel mean radius. The electric field is almost uniform in the radial direction and negligible outside the closed drift region. Therefore, it can be approximated as $E = U_d/l_D$, where l_D is the length of the closed drift region. The drift of electrons in the azimuthal direction gives rise to the *Hall current* which is the integral of the drift velocity, v_E (Eq. 2.17) and the electron plasma density, n_e, over l_D:

$$I_H = n_e e \left(\int_0^{l_D} v_E dz\right) w = n_e e \left(\int_0^{l_D} E/B dz\right) w. \tag{3.2}$$

As we assume $E = U_d/l_D$, the Hall current is approximated by

$$I_H \approx n_e e w U_d/B. \tag{3.3}$$

It can be deduced from this equation that for a fixed magnetic field the Hall current is proportional to the applied discharge voltage and the channel width. In Hall thrusters optimized for high efficiency, the optimal magnetic field is proportional to the discharge voltage [6]. Therefore, from Eq. 3.3 it can be concluded that for a given plasma density or beam current in high-efficiency Hall thrusters, the Hall current is approximately constant.

Although electrons are confined to the closed drift region by the magnetic field, they diffuse to the anode as a result of collisions (see Sec. 2.7). However, as they diffuse at a low rate, electrons emitted by the cathode and the secondary electrons created from the ionization of neutrals continuously replace them such that the quasi-neutrality assumption always holds within the closed drift region [6].

Due to low axial electron current density near the channel exit, the ion current dominates in the closed drift region. Thus, the current is carried mostly by ions, $j_z = j_{iz}$. In the near-anode region, however, the electron current dominates due to low ionization rate and small ion velocity.

In order to create the ionization and acceleration regions as described above, the magnetic field strength must be chosen such that the electrons are confined to closed drift region whereas the ions' motion is not obstructed. The reduction of electrons' mobility necessitates that $\omega_c^2/\nu^2 >> 1$ (See Eq. 2.45). This means that the electrons must be magnetized such that they make many orbits around a field line before a collision with a neutral occurs and results in cross-field diffusion [6]. Accordingly, the electron Larmor radius, r_e, must be much less than the closed drift region length, l_D. If an electron's velocity is characterized by its thermal velocity, v_{th}, the electron Larmor radius is

$$r_e = \frac{v_{th}}{\omega_c} = \frac{m}{eB}\sqrt{\frac{8kT_e}{\pi m}} = \frac{1}{B}\sqrt{\frac{8m}{\pi e}T_{eV}} << l_D. \tag{3.4}$$

For example, the electron Larmor radius at a temperature of 25 eV and a typical radial magnetic field strength of 150 G typical in Hall thrusters is 0.13 cm, which is much smaller than the channel width and plasma length in HETs [6].

On the other hand, the ions must be non magnetized so that their motion is not influenced by the magnetic field and they can be accelerated effectively out of the channel by the electric field. Hence, the length of the closed drift region, l_D, should be significantly less than the Larmor radius for ions, r_i. Taking the maximum ion velocity as in Eq. 3.1, the ion Larmor radius is

$$r_i = \frac{v_i}{\omega_c} = \frac{M}{eB}\sqrt{\frac{2eU_d}{M}} = \frac{1}{B}\sqrt{\frac{2M}{e}U_d} >> l_D. \tag{3.5}$$

For example, r_i, in the 150 G radial field and at 300 V of applied discharge voltage is about 180 cm, which is much larger than the channel or plasma dimensions [6]. To sum up, the magnetic field strength is determined such that the electrons are trapped by the field while the ions are insensitive to it.

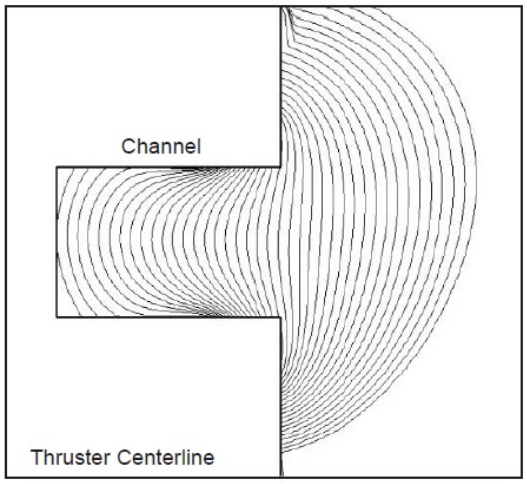

Figure 3.3: Usual magnetic field configuration of a HET [6].

The distribution of the magnetic field lines is also important because their shape controls the ion trajectories. The magnetic field between the anode and the maximum field location should align in the radial direction at the mean diameter of the discharge chamber [31]. In order to focus the ions such that they are accelerated in the axial direction and to minimize their impingement on the inner and outer walls of the discharge channel, the magnetic field strength must be continuously increasing from the anode to the location of maximum strength near the exit plane. Such a configuration results in the curved field lines, concave as seen in Fig. 3.3.

As the equipotential lines approximately follow the shapes of magnetic field lines (explained in Sec 3.6), a field configuration as in Fig. 3.3 allows the focusing of ions away from the channel walls, so that much of the ions can leave the channel without striking a wall. A desirable shape of the magnetic field can be obtained by adjusting the relative strengths of the inner and outer magnet windings.

3.5 Potential and Current Distributions

In HETs, the discharge voltage, U_d, applied between the anode and the cathode typically has the axial profile as shown in Fig. 3.4. In the previous section it has been mentioned that the electric field is nearly zero in the near anode region and peaks toward the channel exit. Accordingly, the potential is almost constant in the weak electric field region then it falls sharply toward the cathode potential near the channel exit (Fig. 3.4). The voltage of the beam,U_b, formed by the exhausted ions and neutralizing electrons is slightly lower than the discharge voltage. The difference between them is called the coupling voltage, U_c, which is required to extract electrons from the cathode.

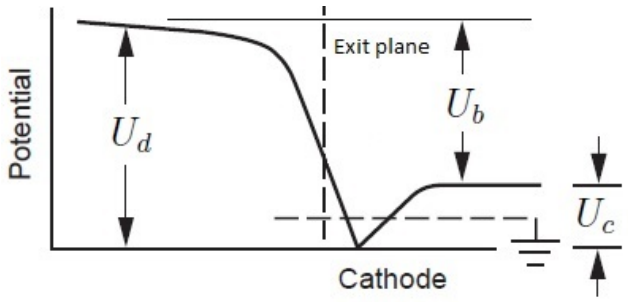

Figure 3.4: Hall thruster potential distribution (adapted from [6]).

The discharge current, I_d (see Fig. 3.5), is the net current flowing through the discharge supply. Ion flux to the anode is very small so the discharge current is almost equal to the the electron current collected by the anode, I_a. Similarly, the discharge current is equal to the electron current emitted by the cathode, I_c, since the ion flux to the cathode is negligible. Hence, the discharge current is approximately $I_d = I_a = I_c$. The ion and electron currents to the channel walls

are equal so the net current to the walls is zero.

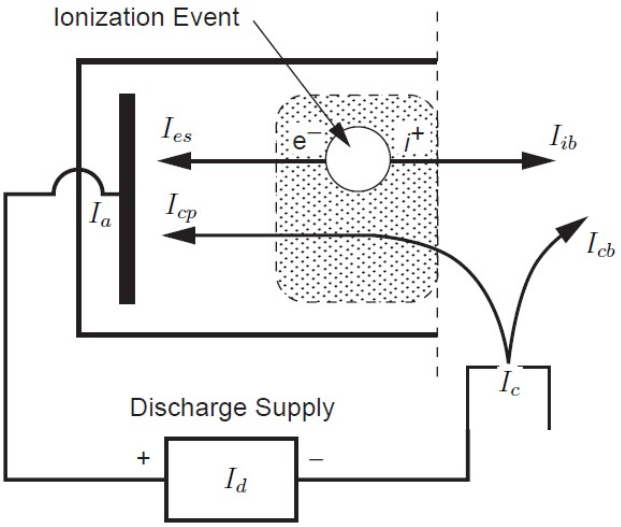

Figure 3.5: Schematic showing the electric currents in the discharge channel of a HET (adapted from [6]).

Some fraction of the electrons flowing to the anode comes from the ionized atoms, I_{es} (secondary electrons) and the other from the cathode I_{cp} (primary electrons). Thus $I_d = I_a = I_{es} + I_{cp}$.

Since in the ionization event, the total charge of the electrons removed from atoms is equal to the total charge of the ions generated, the ion beam current is equal to the secondary electron current to the anode ($I_{ib} = I_{es}$).

Some fraction of the electrons emitted by the cathode neutralizes the ion beam, I_{cb} . Therefore the ion beam current and the neutralizing electron current are equal ($I_{ib} = I_{cb}$) which means that $I_{cb} = I_{es}$.

The total electron current from the cathode is then $I_c = I_{cp} + I_{cb} = I_{cp} + I_{es} = I_a = I_d$. A schematic of the electric currents is shown in the Fig. 3.5.

3.6 Modeling of Hall thrusters

An exact and self-consistent description of a SPT can be done by solving the kinetic Boltzmann equation (Eq. 2.21) for each species with Maxwell's equations (Eq. 2.4) simultaneously [23]. However, complexity of the full description

of real processes in SPTs and therefore the substantial computational load of large number of particles in kinetic approach forces researchers to use some assumptions such as describing the plasma species as fluids instead of particles and reducing the problem to one or two dimensions in space.

Early Hall thruster studies were based predominantly on experiments rather than numerical analyses due to insufficient computational tools available at that time. However, during the past 20 years, numerical models have also evolved. These models can be divided into three main categories: fluid, kinetic and hybrid models.

Some assumptions are common in almost all HET models. First of all, as the time variation of the magnetic field due to moving charges is small compared to the externally applied field, the magnetic field is assumed as static. It is either numerically calculated at the beginning or taken from experimental studies or it is expressed in an approximate analytical form. Since $\partial \mathbf{B}/\partial t = 0$, $\nabla \times \mathbf{E} = 0$ (Eq. 2.4) and the electrostatic approximation is valid, $\mathbf{E} = -\nabla U$. Also, as the ion Larmor radius is much larger than the thruster dimensions, the magnetic force acting on ions is neglected.

In kinetic models, for each plasma species, particle motion is described by the velocity distribution function obtained from the solution of the Boltzmann equation. Although kinetic modeling is advantageous in providing detailed information about the physics of plasma processes, it is not practical due to very large computation time required. Fluid models include continuity, momentum and energy equations which are derived by taking moments of the Boltzmann equation in velocity space (Sec. 2.5). Therefore, plasma properties of interest in fluid models are macroscopic quantities. Although these models are computationally more efficient, they do not represent all the physical aspects adequately. Hybrid modeling, where electrons are modeled as fluid while neutrals and ions are treated as particles, is a compromise between the kinetic and fluid approaches.

In many thruster models, electrons are assumed to have the Maxwellian velocity distribution and treated as fluids. In the fluid formulation, the electron transport is described in the magnetic frame of reference by the Ohm's law (Eq.

2.51), which is derived from the electron momentum equation. There are three components of the resistivity in the direction perpendicular, parallel and transverse to the local magnetic field, which are represented by the subscripts $\perp, \parallel, \wedge$, respectively.

$$\eta \mathbf{j} = \eta_{\perp} \mathbf{j}_{\perp} + \eta_{\parallel} \mathbf{j}_{\parallel} + \eta_{\wedge} \mathbf{j}_{\wedge} \tag{3.6}$$

Along the magnetic field lines, $\mathbf{j} \times \mathbf{B}$ is zero. Therefore, the electric field along the $\mathbf{B}$ field lines is

$$E = -\frac{\nabla p}{en} + \eta j_e + \eta_{ei} j_i = -\nabla u. \tag{3.7}$$

The motion of electrons is not constrained along magnetic field lines. Thus, the electron diffusion coefficient is much higher along field lines than across them. Therefore, it is possible to consider a simple balance of pressure and electric forces along the field lines by $\nabla p = en\nabla U$.

Electrons moving very fast along the field lines reach thermal equilibrium very rapidly. Assuming uniform electron temperature along the field lines, the potential at any point on a given field line is [6]

$$U = U_0 + \frac{kT_e}{e} ln\left(\frac{n}{n_0}\right), \tag{3.8}$$

where U_0 and n_0 are the potential and density at a reference point on a given field line, respectively. The density gradient is relatively small along the field lines, therefore potential is almost constant. Equipotential lines coincide with the magnetic field lines within kT_e/e [6].

Across the magnetic field lines, the perpendicular resistivity can be written in terms of the perpendicular electron mobility:

$$\eta_{\perp} = \frac{1}{en\mu_e} = \frac{1 + {\omega_c}^2/\nu^2}{en\mu_e}. \tag{3.9}$$

Then the perpendicular electron flux can be written from the Ohm's law as

$$j_{e\perp} = \mu_{e\perp}\left(enE_{\perp} + \frac{\partial p_e}{\partial x}\right) - \frac{\nu_{e\perp}}{\nu_{ei}} j_{i\perp}, \tag{3.10}$$

where μ_{ei} is the electron mobility due to only electron-ion collisions.

The collision frequency include both electron-ion and electron-neutral collisions. Measurements show that the electron transport across the magnetic field is higher than that predicted by the classical theory. Two mechanisms play a role in this "anomalous" electron transport. First is the electron wall interactions by which the electron momentum is scattered and secondary electrons are introduced into the channel. This effect is represented by an effective wall scattering frequency. The second is the Bohm diffusion which arises from azimuthal drift instabilities. Using the Bohm diffusion coefficient from Eq. 2.49 and Eq. 2.40 , *Bohm mobility* can be defined as

$$\nu_B = \frac{1}{\gamma B} = \frac{e}{\gamma m \omega_c}, \tag{3.11}$$

where γ is a coefficient adjusted to make the results of the numerical analysis fit the experimental data [6]. The Bohm collision frequency is then $\nu_B = \gamma\omega_c$.

Therefore, the total collision frequency is

$$\nu_m = \nu_{ei} + \nu_{en} + \nu_w + \nu_B. \tag{3.12}$$

The electron energy equation applied in Hall thrusters is derived from the general form of the energy equation 2.27 (see Ref. [6]).

$$\frac{\partial}{\partial t}\left(\frac{3}{2}n_e k T_e\right) + \nabla\cdot\left(\frac{5}{2}n_e k T_e \mathbf{v}_e\right) - \nabla(K_e \nabla T_e) = \mathbf{E}\cdot\mathbf{j}_e - R - S - P_w, \tag{3.13}$$

where $\mathbf{E}\cdot\mathbf{j}_e$ is the ohmic heating, R is the radiative energy loss due to excitation of neutrals, S is the ionization energy loss, and P_w is the electron energy loss to the walls. Note that the electron directed kinetic energy term ($n_e m {v_e}^2$) is omitted since it is small compared to electron thermal energy [20]. The radiative energy loss is $R = U_{ex} n_e n_a \langle\sigma_{ex} v_e\rangle$ and the ionization energy loss is given by $S = U_i n_e n_a \langle\sigma_i v_e\rangle$, where U_{ex} and U_i are the excitation and ionization potentials, respectively.

Contrary to electrons, ions in a Hall thruster have low random velocities and temperatures, but high directed velocities as they are accelerated by the electric field. Therefore they do not reach thermal equilibrium, their velocities and fluxes

tend to be different from Maxwellian distribution. Also, ions are assumed to be collisionless, because electron-ion collisions mean free path is much larger than the discharge channel length [6, 3]. Due to their high directed velocities they leave the channel after a single pass. Therefore the dynamics of the ions is described by the kinetic Boltzmann equation [25]:

$$\frac{\partial f_i}{\partial t} + \mathbf{v}_i \cdot \nabla f_i + \frac{e}{M}(\mathbf{E} + \mathbf{v}_i \times \mathbf{B}) \cdot \nabla_{\mathbf{v}_i} f_i = n_e \sigma_i v_e f_a(\mathbf{v}_i). \tag{3.14}$$

Here, the term on the RHS represent the ion generation. The electron-ion recombination is ignored since the recombination rate is several order of magnitude smaller than the ionization rate [20].

Similarly, the neutral atoms dynamics is described by

$$\frac{\partial f_a}{\partial t} + \mathbf{v}_a \cdot \nabla f_a = -n_e \sigma_i v_e f_a(\mathbf{v}_i). \tag{3.15}$$

Then, the ion number density and the ion current are calculated by the following integrals:

$$n_i(\mathbf{r}, t) = \int_{-\infty}^{\infty} f_i(\mathbf{r}, \mathbf{v}_i, t) d\mathbf{v}_i, \qquad \mathbf{j}_i(\mathbf{r}, t) = e \int_{-\infty}^{\infty} \mathbf{v}_i f_i(\mathbf{r}, \mathbf{v}_i, t) d\mathbf{v}_i. \tag{3.16}$$

3.7 Survey of Numerical Models

Fluid models consider all species to have Maxwellian velocity distribution. Ions are typically assumed as cold (ion thermal pressure is neglected) and electrons have a single temperature. Fluid codes are very fast and they have been applied for both 1-D and 2-D axisymmetric geometries and both stationary and time-dependent solutions. A 1-D steady-state model including the anode sheath region and the plume region near the exit plane was developed by *Ahedo et al.* [7]. 2-D models were developed by Roy and Pandey [26], *S.Barral* [27] and *Mikellides et al.* [10].

The kinetic approach allows to handle the non-Maxwellian distribution functions expected in Hall thrusters. Therefore, the accuracy of the results is improved, but at the expense of greater computational cost. In such models, kinetic equations are typically solved using particle-in-cell (PIC) method while collisions are

modeled by Monte-Carlo (MCC) method. In the PIC-MCC method, plasma species are represented by discrete macro-particles in each cell. The algorithm is as follows: Electric charges are distributed to the computation domain. The electric potential is calculated from the Poisson equation. Having determined the electric field, particles are propagated. Then for each macro-particle, collision probability is calculated by using the cross-section data for various type of collisions and comparing it to a random number. If the collisions result in ionization, new particles are introduced to the system. The new charge distribution is calculated and the whole procedure is repeated. Electrons move on a much smaller timescales than ions and neutral atoms. Thus, timesteps for electrons are two order of magnitude smaller than timesteps for heavy particles. Several kinetic models have been developed by *M.Hirakawa and Y.Arakawa* [9], *Szabo* [11], *Gorshkov et al.* [28] and Taccogna [29].

Hybrid models, by considering heavy species as particles and electrons as a fluid, combine the accuracy of the kinetic models and speed of the fluid models. The hybrid codes were pioneered by M.Fife [20]. In his 2-D model he used the PIC treatment for heavy particles. For electrons, he used the thermalized potential concept (Eq. 3.8), therefore he reduced the 2-D problem to a quasi 1-D problem. Having determined first the thermalized potential values for each individual field lines, he calculated the potentials at grid points along those lines. This approach was also adopted in models by *Komurasaki and Arakawa* [16], *Garrigues et al.* [17] and *Koo* [13]. Besides these 2-D models, there exist also many 1-D hybrid codes which are simpler but which can good results to some extent. Some examples of them are the models developed by Lentz [4], Boeuf [3], *Morozov and Savelyev* [23], *Hara and Boyd* [15]. In these models, kinetic Vlasov equation for ions is directly solved instead of using a PIC algorithm.

CHAPTER 4

ONE DIMENSIONAL FLUID AND HYBRID MODELS

In this thesis, a numerical analysis of the plasma properties in the discharge channel of a Hall thruster is carried out, based on a physical model by A. I. Morozov [23, 24, 22, 21]. In this chapter, the model is presented: the assumptions, governing equations and boundary conditions are explained in detail. Then, the non-dimensional forms of the governing equations are derived.

Our model is one dimensional so that plasma variables are uniform in the radial and azimuthal directions but change in the axial direction ($x - axis$) along the discharge channel (as in the models in references [4, 3, 23, 15]). The computational domain is bounded by the anode surface (at the base of the channel) ($x = 0$) and the channel exit ($x = L$) where the cathode is placed.

Xenon is used as the propellant. Three species are considered in the model: Xe atoms, Xe^+ ions and electrons. Although it is known from experiments that doubly charged xenon ions, Xe^{+2}, also exist in the channel, they are neglected in this model due to their low concentration (see Sec 3.4). Ions are insensitive to the magnetic field since their Larmor radius is much greater than the channel dimensions (Eq. 3.5) and they leave the discharge channel without colliding with other particles [3].

Xe atoms are injected into the discharge channel with a velocity v_a. Since no force is acting on them, they move with this constant velocity along the channel [3]. Therefore momentum equation for neutral atoms is eliminated.

Another assumption in the model is quasi-neutrality. Everywhere along the

discharge channel, ion and electron number densities are assumed to be equal, $n_i \approx n_e$. Therefore, both densities are denoted by n. The axial electric field is not obtained from Poisson's equation but is calculated from Ohm's law.

It was explained in Sec. 3.6 that in Hall thrusters, magnetic field induced by the motion of charged particles is small compared to externally applied magnetic field. Therefore, the magnetic field is assumed to be static and approximated analytically.

4.1 Fluid approach

4.1.1 Governing equations

The governing equations of the fluid model are taken from the model by Morozov [23, 24] and they can be derived from the macroscopic transport equations given in Sec. 2.5.

- *the ion continuity equation*

  Eq. 2.25 can be written for ions in one dimension as

  $$\frac{\partial n}{\partial t} + \frac{\partial nv}{\partial x} = \beta n n_a, \tag{4.1}$$

  where v is the ion velocity and n_a is the neutral density. The source term on the right-hand side (RHS) represents the ion generation. β is the ionization rate coefficient.

- *the ion momentum equation*

  Since the ions are assumed as cold and collisionless, the second and third terms in the momentum equation (Eq. 2.26) are dropped. Also, ion loss to the channel walls is not taken into account. Therefore, the momentum equation for ions is

  $$\frac{\partial nv}{\partial t} + \frac{\partial nv^2}{\partial x} = \frac{en}{M}E + \beta n n_a v_a. \tag{4.2}$$

  Here M is the mass of a Xe atom. The second term on the RHS represents the momentum contribution by the ionized atoms having a velocity v_a before ionization.

Multiplying Eq. 4.1 with v and substracting it from Eq. 4.2, the ion momentum equation can also be written as

$$\frac{\partial v}{\partial t} + v\frac{\partial v}{\partial x} = \frac{eE}{M} + \beta n_a(v_a - v). \tag{4.3}$$

- *the neutral atom continuity equation*

$$\frac{\partial n_a}{\partial t} + v_a\frac{\partial n_a}{\partial x} = -\beta n n_a. \tag{4.4}$$

As mentioned before, the neutral atom velocity, v_a, is constant throughout the channel. The term on the RHS represents the neutral atom depletion due to ionization.

- *Ohm's law*

The electron dynamics is governed by the Ohm's law (Eq. 2.51) derived from the electron momentum equation. Neglecting electron diffusion ($\nabla p = 0$) and electron-ion collisions ($\nu_{ei} = 0$), Ohm's law can be written in a simplified form as

$$E = \frac{j_e}{\sigma(x)} = \frac{J - j_i}{\sigma(x)}, \tag{4.5}$$

where J, j_e and j_i are the discharge, electron and ion currents (per area), respectively. The ion current density is $j_i = env$ and $\sigma(x)$ is the plasma conductivity which is the inverse of the resistivity. According to the classical transport theory, $\sigma(x) \sim 1/B^2$ (see Sec. 2.7), and it is defined in [21] as

$$\sigma(x) = \sigma_0 \left[\frac{B_0}{B(x)}\right]^2, \quad \sigma_0 = const, \quad B_0 = const. \tag{4.6}$$

Here B_0 is the magnetic field strength at the anode surface and $B(x)$ is the profile of the magnetic field which is approximated in [24] as a parabolic function of the axial position:

$$B(x) = B_0[b_0 + (1 - b_0)(x/L)^2], \tag{4.7}$$

where $b_0 = B(0)/B_0$.

- *the equation of the electric circuit*

Finally, the equation of the electric circuit is given by

$$L_c\frac{dJ}{dt} + RJ + \int_0^L E dx = U_0. \tag{4.8}$$

Here U_0 is the applied discharge voltage (It was denoted by U_d in the previous chapters), L_c is the inductance and R is the resistance of the circuit.

The boundary conditions at the anode surface are

$$n(0,t) = n_0,\ n_a(0,t) = n_{a0},\ v(0,t) = v_0, \tag{4.9}$$

where constants n_0, n_{a0}, v_0 will be defined later on.

4.1.2 Non-dimensionalization of the fluid model equations

In order to simplify the problem, dimensionless form of the variables is introduced. Dimensionless equations containing new variables are derived from the original equations 4.1-4.8. In the application of the non-dimensionalization process, the channel length L is taken as a unit of length. Then $E_0 = U_0/L$ is a unit of the electric field and $J_0 = U_0/R_0$ a unit of the electric current density, where $R_0 = L/\sigma_0$ is the resistivity of the channel with a cross-section of $S = 1$ m^2. The neutral density at the anode n_{a0} is taken as a unit density for both neutrals and ions. Similarly, the ion velocity at the anode, v_0, is taken as a unit velocity for both neutrals and ions. The unit time is the unit length over the unit velocity, $t_0 = L/v_0$.

Using the unit quantities mentioned above, new non-dimensional variables are defined according to the relation $\hat{p} = p/p_0$, where p is the physical variable, p_0 is the unit quantity and $\hat{p}$ is the nondimensional variable.

Then, a new set of equations is obtained. Substituting $n = \hat{n}n_{a0}$, $n_a = \hat{n}_a n_{a0}$, $x = \hat{x}L$ and $t = \hat{t}t_0 = \hat{t}L/v_0$ into Eq. 4.1, the ion continuity equation becomes

$$\frac{v_0 n_{a0}}{L}\frac{\partial \hat{n}}{\partial \hat{t}} + \frac{n_{a0}v_0}{L}\frac{\partial \hat{n}\hat{v}}{\partial \hat{x}} = \beta n_{a0}^2 \hat{n}\hat{n}_a.$$

Then, multiplying both sides with $L/v_0 n_{a0}$, we obtain

$$\frac{\partial \hat{n}}{\partial \hat{t}} + \frac{\partial \hat{n}\hat{v}}{\partial \hat{x}} = \frac{\beta n_{a0} L}{v_0}\hat{n}\hat{n}_a.$$

Similarly, the neutral continuity equation (Eq. 4.4) has the dimensionless form

$$\frac{\partial \hat{n}_a}{\partial \hat{t}} + \hat{v}_a\frac{\partial \hat{n}_a}{\partial \hat{x}} = -\frac{\beta n_{a0} L}{v_0}\hat{n}\hat{n}_a. \tag{4.10}$$

Substituting $E = U_0\hat{E}/L$ into Eq. 4.3 and using the non-dimensional variables mentioned above, the ion momentum equation becomes

$$\frac{\partial \hat{v}}{\partial \hat{t}} + \hat{v}\frac{\partial \hat{v}}{\partial \hat{x}} = \frac{eU_0}{Mv_0^2}\hat{E} + \frac{\beta n_{a0} L}{v_0}(\hat{v}_a - \hat{v}). \tag{4.11}$$

Inserting $\sigma_0 = L/R_0$ and $J = \hat{J}U_0/R_0$ into Eq. 4.5, the Ohm's Law can be written as

$$\hat{E}\frac{U_0}{L} = \frac{\hat{J}\frac{U_0}{R_0} - e\hat{n}n_{a0}\hat{v}v_0}{\frac{L}{R_0}\frac{1}{[\hat{B}(\hat{x})]^2}}. \tag{4.12}$$

Multiplying both sides by L/U_0, the non-dimensional electric field becomes

$$\hat{E} = \left[\hat{J} - \frac{en_{a0}v_0R_0}{U_0}\hat{n}\hat{v}\right][\hat{B}(\hat{x})]^2. \tag{4.13}$$

Similarly, the equation of the electric circuit (Eq. 4.8) transforms into

$$\frac{L_c U_0 v_0}{LR_0}\frac{d\hat{J}}{d\hat{t}} + rR_0\frac{U_0}{R_0}\hat{J} + \int_0^1 \left(\frac{U_0\hat{E}}{L}\right) L d\hat{x} = U_0,$$

where r is the non-dimensional circuit resistance and R is replaced by rR_0. Dividing both sides by U_0, the circuit equation becomes

$$\frac{L_c v_0}{LR_0}\frac{d\hat{J}}{d\hat{t}} + r\hat{J} + \int_0^1 \hat{E} d\hat{x} = 1.$$

For convenience, the following dimensionless parameters are defined:

$$\mu = \frac{eU_0}{Mv_0{}^2},\ \nu = \frac{\beta n_{a0}L}{v_0},\ \chi = \frac{en_{a0}v_0R_0}{U_0},\ l = \frac{L_c v_0}{LR_0},\ r = \frac{R}{R_0}. \tag{4.14}$$

Using these parameters, the following set of five non-dimensional equations with five unknowns $(\hat{n}, \hat{n}_a, \hat{v}, \hat{E}, \hat{J})$ is obtained:

$$\begin{aligned}
\frac{\partial \hat{n}}{\partial \hat{t}} + \frac{\partial \hat{n}\hat{v}}{\partial \hat{x}} &= \nu\hat{n}\hat{n}_a, \\
\frac{\partial \hat{v}}{\partial \hat{t}} + \hat{v}\frac{\partial \hat{v}}{\partial \hat{x}} &= \mu\hat{E} + \nu\hat{n}_a(\hat{v}_a - \hat{v}), \\
\frac{\partial \hat{n}_a}{\partial \hat{t}} + \hat{v}_a\frac{\partial \hat{n}_a}{\partial \hat{x}} &= -\nu\hat{n}\hat{n}_a,
\end{aligned} \tag{4.15}$$

$$\hat{E} = [\hat{B}(\hat{x})]^2(\hat{J} - \chi\hat{n}\hat{v}),$$
$$l\frac{d\hat{J}}{d\hat{t}} + r\hat{J} + \int_0^1 \hat{E}d\hat{x} = 1.$$

The magnetic field in the dimensionless form is $\hat{B} = B(x)/B_0$ (adopted from [23]) and represented by the following analytical expression:

$$\hat{B}(\hat{x}) = b_0 + (1 - b_0)(\hat{x})^2, \tag{4.16}$$

where $b_0 = B(0)/B_0$.

The inputs to the numerical code are the xenon flow rate, $\dot{m}$, within the range $2.5 - 5$ mg/s, and the discharge voltage, U_0, within the range $300 - 500$ V. The channel length is $L = 3$ cm and the unit time is $t_0 = 15$ μs. The ionization rate parameter, β, is taken as $\beta \simeq 5 \times 10^{-14}$ m^3/s which is the ionization rate of Xe at $T_e = 15$ eV (the average electron temperature in the discharge channel). The neutral atom velocity at the anode is $v_a = 200$ m/s. Then for a channel cross-sectional area of $A = 25$ cm^2, the neutral atom number density is calculated from $n_{a0} = \dot{m}/MAv_a$ as $n_{a0} = 3 \times 10^{19}$ m^{-3} [3].

The value of the channel resistivity, R_0, is estimated by Morozov as $R_0 \simeq 8$ Ω m^2, such that it results in a stationary solution with a total discharge current of $I_d = 3$ A under $U_0 = 300$ V discharge voltage and thus ensures a good agreement with the experimental results. The parameters l, r and b_0 are estimated experimentally as $l \simeq 10^{-2}, r \simeq 10^{-3}, b_0 = 0.1$ [23] and we use the same values in our model.

4.2 Hybrid approach

4.2.1 Governing equations

In the hybrid model, ions are treated kinetically using an ion velocity distribution function (VDF), $f(x, v, t)$. 1D-1V (one dimensional in coordinate space and in velocity space) Vlasov equation (2.22) describes ion motion.

Neutral atoms and electrons are treated as fluid. The electron energy equation is also included in the model in order to understand the role of the electron heat

conduction. As only the electron temperature is considered in this model, it is denoted by T without the subscript e. The ionization rate, β, is now expressed as a function of the electron temperature.

The equations of the hybrid model are [22]:

- *the ion kinetic equation*

$$\frac{\partial f}{\partial t} + v\frac{\partial f}{\partial x} + \frac{eE}{M}\frac{\partial f}{\partial v} = \beta(T)nn_a\delta(v - v_a). \tag{4.17}$$

  The right-hand side represents the ion production. δ denotes the Dirac delta function. It is assumed that the newly generated ions are introduced with a velocity equal to the neutral atoms velocity v_a [3].

- *the neutral atom continuity equation*

$$\frac{\partial n_a}{\partial t} + v_a\frac{\partial n_a}{\partial x} = -\beta(T)nn_a. \tag{4.18}$$

- *the electron energy equation*,

$$\frac{3}{2}\frac{\partial nT}{\partial t} + \frac{5}{2}\frac{\partial nv_eT}{\partial x} = \frac{\partial}{\partial x}\left(\kappa_e\frac{\partial T}{\partial x}\right) + j_eE - \alpha\beta(T)nn_a. \tag{4.19}$$

  On the RHS, the first term describes the heat conduction, the second the joule heating, the third the energy spent for ionization.

- *Ohm's law* (Eq. 4.5)

- *the equation of the electric circuit* (Eq. 4.8)

The macroscopic quantities such as the ion number density n used in Eq. 4.17, 4.18, and the ion current density j_i used in Eq. 4.5 are calculated from the ion velocity distribution function $f(x, v, t)$:

$$n = \int_{-\infty}^{\infty} f(v)dv, \qquad j_i = e\int_{-\infty}^{\infty} vf(v)dv. \tag{4.20}$$

The electron velocity, v_e, in Eq. 4.19 is

$$v_e = -\frac{j_e}{en} = -\frac{J - j_i}{en}. \tag{4.21}$$

The boundary conditions of the hybrid model are [23]:

1- *at the anode surface,* $x = 0$

$$n_a(0,t) = n_{a0}, \qquad \partial T/\partial x = 0, \qquad f(0,v,t) = f_0(v) \ \text{ for } v > 0. \tag{4.22}$$

2- *at the channel exit,* $x = L$

$$T = T_0. \tag{4.23}$$

The ion distribution function at the anode surface is taken in the form [23]:

$$f_0(v) = \frac{\pi}{2}\frac{n_0}{{v_0}^2} v \; exp\left[-\frac{\pi}{4}\left(\frac{v}{v_0}\right)^2\right]. \tag{4.24}$$

The magnetic field, the plasma conductivity and the neutral velocity are set to the same values used in the fluid model.

The ionization rate parameter β is a function of the electron temperature (see Sec 3.4) and it is given in Appendix A. As seen in Fig. A.1, β increases almost linearly with the electron temperature. In [22] β is approximated as

$$\beta(T) = \begin{cases} 0 & \text{if } T < T^+ \\ \beta_0(T/T^+ - 1) & \text{if } T \geq T^+ \end{cases}$$

with $\beta_0 = 2.2 \times 10^{-14}$ m^3/s and $T^+ = 4$ eV. The ion production cost and the electron temperature at the channel exit are indicated in [23] as $\alpha = 40$ eV and $T_0 = 20$ eV, and set to the same values in our model.

The electron heat conduction coefficient, κ_e, is taken as a function of the electron temperature and the magnetic field,

$$\kappa_e = \kappa_{e0}\frac{T}{B}, \tag{4.25}$$

where $\kappa_{e0} = const$ [23].

4.2.2 Non-dimensionalization of the hybrid model equations

The procedure of non-dimensionalization, used earlier in the fluid model, is applied to the hybrid model. Note that $f = n_{a0}\hat{f}$ since function f is related to the particle number density.

In addition to the dimensionless parameters given in Eq. 4.14, two new parameters arise, which are

$$\zeta = \frac{eU_0}{T_0}, \qquad \kappa = \frac{\kappa_{e0}}{Lv_0 n_{a0}}. \tag{4.26}$$

Introducing the dimensionless parameters and variables, the Vlasov equation becomes

$$\frac{\partial \hat{f}}{\partial \hat{t}} + \hat{v}\frac{\partial \hat{f}}{\partial \hat{x}} + \mu \hat{E}\frac{\partial \hat{f}}{\partial v} = \hat{\beta}(T)\nu \hat{n}\hat{n}_a \delta(\hat{v} - \hat{v}_a), \tag{4.27}$$

where $\hat{\beta}(T) = \beta(T)/\beta_0$ and β in the parameter ν (Eq. 4.14) is replaced by β_0. δ function is taken in the dimensionless form as

$$\delta(\hat{v} - \hat{v}_a) = \frac{1}{\sqrt{\pi}\hat{v}_a} exp\left[-\left(\frac{\hat{v} - \hat{v}_a}{\hat{v}_a}\right)^2\right]. \tag{4.28}$$

The dimensionless boundary condition for the ion velocity distribution function is

$$\hat{f}_0(\hat{v}) = \frac{\pi}{2}\frac{\hat{n}_0}{\hat{v}_a^2}\hat{v}\ exp\left[-\frac{\pi}{4}\left(\frac{\hat{v}}{\hat{v}_0}\right)^2\right]. \tag{4.29}$$

Ion density and current given by Eq. 4.20 become

$$\hat{n} = \int_{-\infty}^{\infty} \hat{f}(\hat{v})d\hat{v}, \qquad \hat{j}_i = \chi \int_{-\infty}^{\infty} \hat{v}\hat{f}(\hat{v})d\hat{v}. \tag{4.30}$$

The neutral atom continuity equation in non-dimensional form is

$$\frac{\partial \hat{n}_a}{\partial \hat{t}} + \hat{v}_a\frac{\partial \hat{n}_a}{\partial \hat{x}} = -\hat{\beta}(T)\nu \hat{n}\hat{n}_a. \tag{4.31}$$

The dimensionless electric field is

$$\hat{E} = [\hat{B}(\hat{x})]^2(\hat{J} - \chi \hat{n}\hat{v}).$$

Finally, the electron energy equation becomes

$$\frac{3}{2}\frac{\partial \hat{n}\hat{T}}{\partial \hat{t}} + \frac{5}{2}\frac{\partial \hat{n}\hat{v}_e\hat{T}}{\partial \hat{x}} = \kappa\frac{\partial}{\partial \hat{x}}\left(\frac{\hat{T}}{\hat{B}}\frac{\partial \hat{T}}{\partial \hat{x}}\right) + \frac{\zeta}{\chi}\hat{j}_e\hat{E} - \hat{\alpha}\hat{\beta}(T)\nu \hat{n}_a\hat{n}, \tag{4.32}$$

where $\hat{\alpha} = \alpha/T_0 = 2$ and $\kappa = 1$ as given in [23].

CHAPTER 5

NUMERICAL SOLUTION AND RESULTS

In this chapter, the solution procedure of the governing equations given in the previous chapter is described. The equations are solved by applying finite difference schemes. Numerical codes for both stationary and transient solutions are developed using Matlab software [19].

5.1 Fluid model

5.1.1 Stationary solution

In order to find the stationary solution, time derivatives in Eq. 4.15 are eliminated and the following system of equations is obtained:

$$\begin{aligned}
\frac{\partial \hat{n}\hat{v}}{\partial \hat{x}} &= \nu \hat{n}\hat{n}_a, \\
\hat{v}\frac{\partial \hat{v}}{\partial \hat{x}} &= \mu \hat{E} + \nu \hat{n}_a(\hat{v}_a - \hat{v}), \\
\hat{v}_a\frac{\partial \hat{n}_a}{\partial \hat{x}} &= -\nu \hat{n}\hat{n}_a, \\
\hat{E} &= [\hat{B}(\hat{x})]^2(\hat{J} - \chi \hat{n}\hat{v}), \\
(r + r_0)\hat{J} - \chi \int_0^1 [\hat{B}(\hat{x})]^2 \hat{n}\hat{v} d\hat{x} &= 1.
\end{aligned} \tag{5.1}$$

Here $r_0 = \int_0^1 [\hat{B}(\hat{x})]^2 d\hat{x}$. Now, let's remove the $\hat{}$ notation on the non-dimensional variables for the sake of simplicity and introduce $C = \mu E + \nu v_a n_a$. Rearranging

the first two equations in 5.1, the derivatives of the ion density and velocity can be written as

$$\frac{\partial n}{\partial x} = \frac{2\nu n n_a}{v} - \frac{nC}{v^2}, \qquad \frac{\partial v}{\partial x} = \frac{C}{v} - \nu n_a. \tag{5.2}$$

From the ion and neutral continuity equations in Eq. 5.1, it is obvious that

$$\frac{\partial nv}{\partial x} = -v_a \frac{\partial n_a}{\partial x}. \tag{5.3}$$

Integrating both sides, the following equation is obtained:

$$v_a n_a + nv = n_0 v_0 + n_{a0} v_a = n_0 + v_a. \tag{5.4}$$

Note that the non-dimensional v_0 and n_{a0} are equal to 1. Using this algebraic equation, the differential neutral continuity equation is eliminated from the system.

Let $r_1 = \int_0^1 [B(x)]^2 nv dx$. The discharge current density in terms of r_0 and r_1 is

$$J = \frac{1 + \chi r_1}{r + r_0}. \tag{5.5}$$

Stationary solution is obtained using the Euler method on a uniform grid with 320 nodes. This number is determined by trial-and-error such that the convergence of the solution is ensured. The solution procedure is iterative. First, an initial estimation for J is introduced. Using this value, E and C are calculated at the left boundary (at the anode surface). Then, ion density and velocity are calculated step by step from Eq. 5.2 at each grid point:

$$n_{i+1} = n_i + \Delta x \left(\frac{2\nu n_i n_{ai}}{v_i} - \frac{n_i C_i}{v_i^2} \right), \tag{5.6}$$

$$v_{i+1} = v_i + \Delta x \left(\frac{C_i}{v_i} + \nu n_{ai} \right). \tag{5.7}$$

Simultaneously, n_a, E and C are evaluated:

$$n_{ai} = \frac{n_0 + v_a - n_i v_i}{v_a},$$

$$E_i = [B(x_i)]^2(J - \chi n_i v_i),$$

$$C_i = \mu E_i + \nu n_{ai} v_a.$$

After n, n_a, v and E are found at each grid point, J is updated from Eq. 5.5 where r_0 and r_1 are calculated by the trapezoidal rule. Then n, n_a, v and E are recalculated. These iterations are repeated until J converges:
$(J^{new} - J^{old})/J^{new} < Tol$, where $Tol = 10^{-3}$.

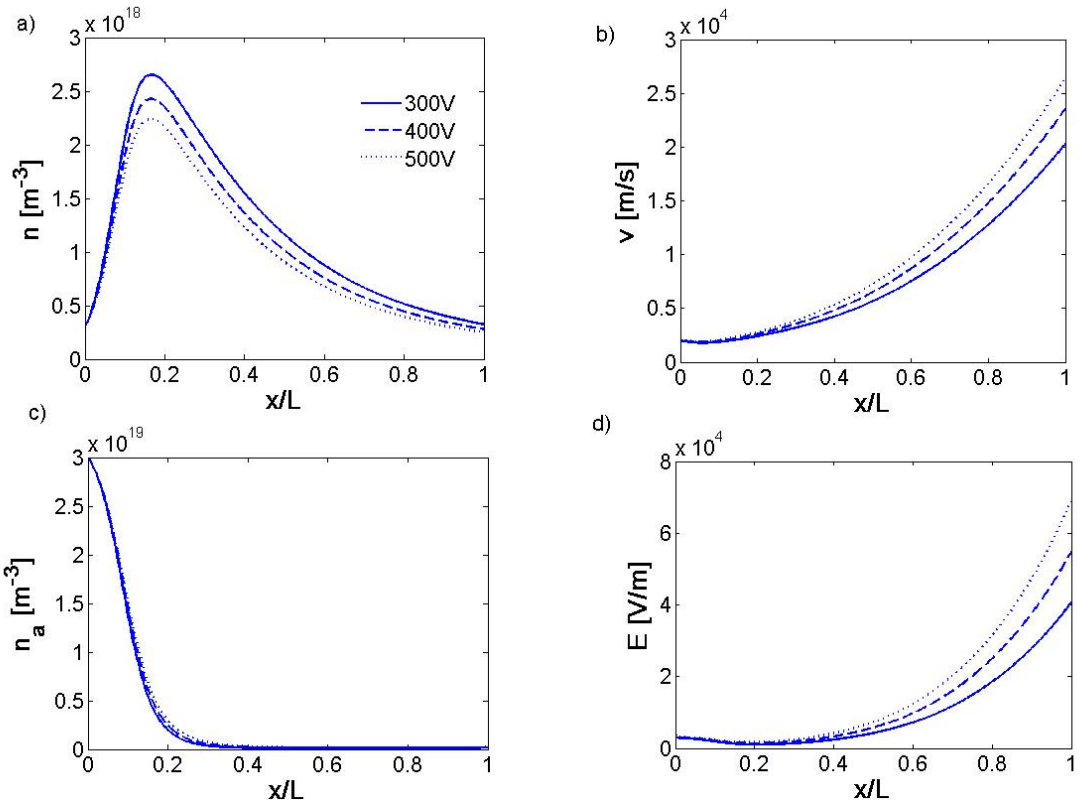

Figure 5.1: Fluid model stationary solution: (a) ion number density, (b) neutral atom number density, (c) ion velocity and (d) electric field profiles along the discharge channel obtained under different discharge voltages for $\dot{m} = 3.25$ mg/s.

Figure 5.1 shows the axial profiles of the main thruster parameters. The profiles are obtained for different discharge voltages, $U_0 = 300 - 500\ V$, while the propellant flow rate is held constant, $\dot{m} = 3.25$ mg/s. At $x/L \simeq 0.2$, the ion number density reaches its maximum which is $(7.5 - 9) \times n_0$ for the given range of the input discharge voltages. At $x/L = 0.25$, atoms are depleted, the propellant gas is almost fully ionized. Then the flow accelerates to an average velocity of

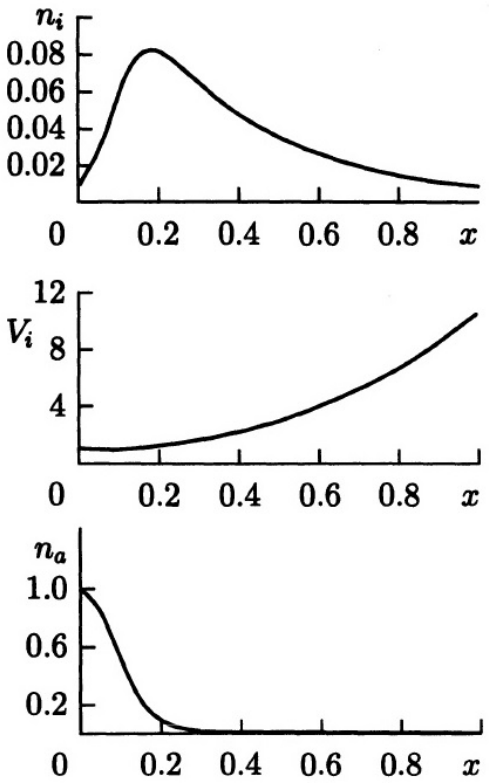

Figure 5.2: The ion density and velocity and neutral atom density distributions obtained in a stationary model with $\dot{m} = 3\ mg/s$, $U_0 = 400V$ [23].

$(10 - 12) \times v_0$ at the channel exit. As can be seen in Fig. 5.1, the electric field and the ion velocity curves shift upwards with increasing discharge voltage. The profile of the atom number density remains almost the same at different discharge voltage regimes. Actually, the profiles plotted in Figure 5.1 are in good agreement with the results found in [23] and demonstrated in Fig. 5.2 where the ion velocity at the channel exit plane is $v_{ex} = 10\ v_0$ and the maximum ion density in the channel is $n_{max} = 8\ n_0$ for $U_0 = 400\ V$ and $\dot{m} = 3\ mg/s$.(Vertical axes in Fig. 5.2 correspond to the non-dimensional ion density, ion velocity and neutral atom density, respectively).

As almost all the neutral atoms become ionized towards the channel exit, only ions contribute to the thrust, which can be expressed as

$$T = \dot{m} v_{ex}. \tag{5.8}$$

The efficiency is defined as the ratio of jet power to the input power [6]. The

jet power is $P_{jet} = T^2/2\dot{m}$. As most of the power is used for the discharge, the discharge power P_d may be taken as the input power P_{in} [14]. Therefore, the efficiency becomes

$$\eta = P_{jet}/P_{in} = \frac{T^2}{2\dot{m}P_d}, \tag{5.9}$$

where $P_d = I_d U_d$.

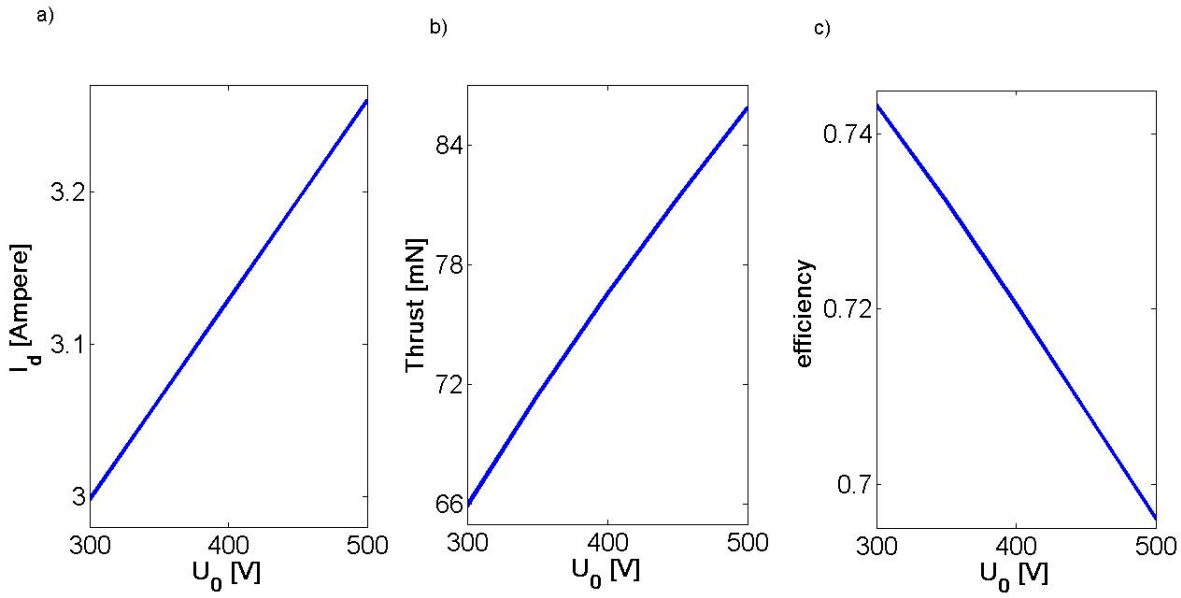

Figure 5.3: (a) The discharge current I_d, (b) the thrust T and (c) the efficiency η versus the discharge voltage U_0.

Figure 5.3 shows the dependence of the discharge current, the thrust and the efficiency on the discharge potential. There is a linear relationship between the discharge current and voltage. The thrust increases with the discharge voltage but this cannot compensate for the high discharge power input which results in a decrease in thruster efficiency. Results illustrated in Fig. 5.3 agree well with those from [24].

5.1.2 Transient solution and oscillation regimes

The stability of the stationary solutions is studied by taking them as initial conditions for the time dependent equations. Time evolutions of plasma variables are calculated using the first order upwind scheme [32] on the same uniform grid used in the stationary solution. Time step is determined according to Courant–Friedrichs–Lewy (CFL) condition:

$$\Delta t = C\frac{\Delta x}{max(v)}, \tag{5.10}$$

where $C \leq 1$ and Δt is updated at each time iteration as $max(v)$ (the maximum value of the ion velocity in the discharge channel) changes with time.

In the transient solution, for numerical stability, an upwind scheme is used. At the new time step $k+1$, n_i and v_i are updated by using the values from the previous time step k using the following finite difference equations:

If $v_i \geq 0$:

$$n_i^{k+1} = n_i^k - \frac{\Delta t}{\Delta x}(v_i^k n_i^k - v_{i-1}^k n_{i-1}^k) + \Delta t(\nu n_i^k {n_a}_i^k), \tag{5.11}$$

$$v_i^{k+1} = v_i^k - \frac{\Delta t}{\Delta x} v_i^k (v_i^k - v_{i-1}^k) + \Delta t(\mu E_i^k + \nu {n_a}_i^k (v_a - v_i^k)). \tag{5.12}$$

If $v_i < 0$:

$$n_i^{k+1} = n_i^k - \frac{\Delta t}{\Delta x}(v_{i+1}^k n_{i+1}^k - v_i^k n_i^k) + \Delta t(\nu n_i^k {n_a}_i^k), \tag{5.13}$$

$$v_i^{k+1} = v_i^k - \frac{\Delta t}{\Delta x} v_i^k (v_{i+1}^k - v_i^k) + \Delta t(\mu E_i^k + \nu {n_a}_i^k (v_a - v_i^k)). \tag{5.14}$$

n_{ai} is updated by backward difference scheme, since v_a is a constant and always positive:

$${n_a}_i^{k+1} = {n_a}_i^k - \frac{\Delta t}{\Delta x} v_a ({n_a}_i^k - {n_a}_{i-1}^k) - \Delta t(\nu n_i^k {n_a}_i^k). \tag{5.15}$$

The electric field is updated using the new values of n and v:

$$E_i^{k+1} = [B(x_i)]^2 (J - \chi n_i^{k+1} v_i^{k+1}). \tag{5.16}$$

After having calculated new values of n, v, n_a and E at each grid point, the discharge current density J is updated from the circuit equation:

$$J^{k+1} = J^k + \frac{\Delta t}{l}\left(1 - \sum_{i=1}^{i_{max}} \frac{E_i^k + E_{i+1}^k}{2}\Delta x - rJ^k\right), \tag{5.17}$$

where i_{max} is the total number of grid points.

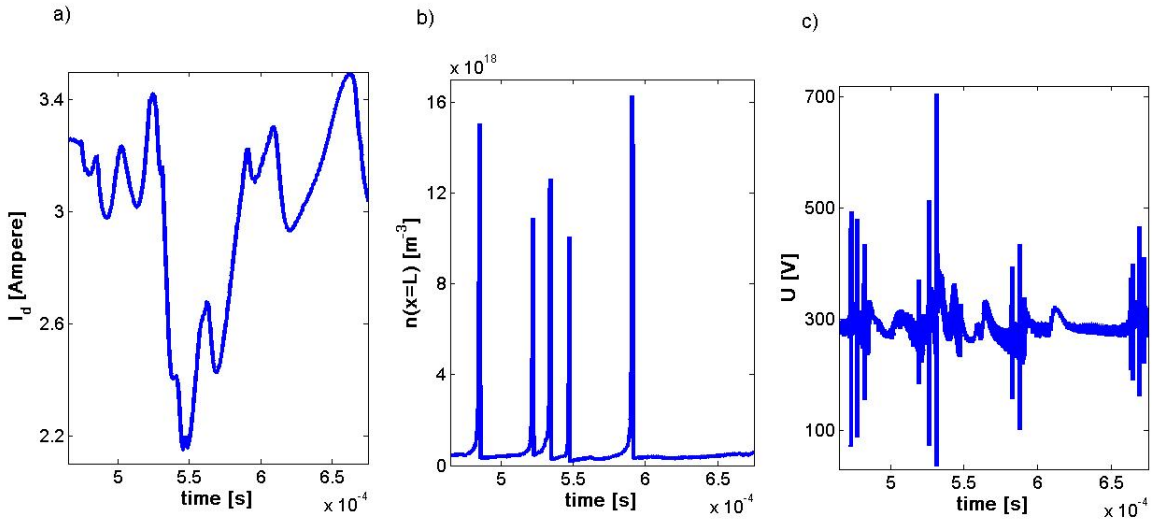

Figure 5.4: Time evolutions of (a) $I_d(t)$, (b) $n(x = L, t)$, (c) $U(t)$ in the aperiodic regime for $U_0 = 300$ V ($\chi = 255$).

The stationary solution for $U_0 = 300$ V is found to be unstable and oscillations of the discharge current $I_d(t)$, the ion number density at the channel exit $n(x = L)$ and the channel voltage $U(t)$ ($= \int E dx$) are aperiodic as seen in Figure 5.4.

Morozov explains in [23] that the behavior of the transient solution in his fluid model depends on the parameter, χ, which is inversely proportional to the discharge voltage (4.14). He states that for sufficiently small values of χ, a stationary stable solution can be found. Increasing χ, a periodic solution emerges. If χ is increased further, the solution becomes unsteady and oscillations of the plasma variables become aperiodic. Actually the last case corresponds to the discharge voltages within the range of practical interest ($U_0 = 200 - 600$ V).

In order to see the effect of the parameter χ as mentioned in [23], the discharge voltage is increased to large values even though the fact that these high values are not realistic for the operation conditions of Hall thrusters. Figure 5.5 (1) and (2) present the evolutionary behavior of $I_d(t)$, $n(x = L, t)$ and $U(t)$ for χ values of 38 and 16 which correspond to discharge voltages 2000 and 4800 V respectively for a channel resistivity of $R_0 \simeq 8\ \Omega\ \mathrm{m}^2$. Oscillations are periodic in the first case and damped in the second confirming that solution becomes stable with sufficiently decreased χ. These results are consistent with those found by Morozov (see Fig. 5.6) where periodic and non-periodic oscillations were observed for $\chi = 45$ and $\chi = 175$, respectively. In Fig. 5.6, vertical axes correspond to the non-dimensional discharge current, channel voltage and the ion density at the channel exit.

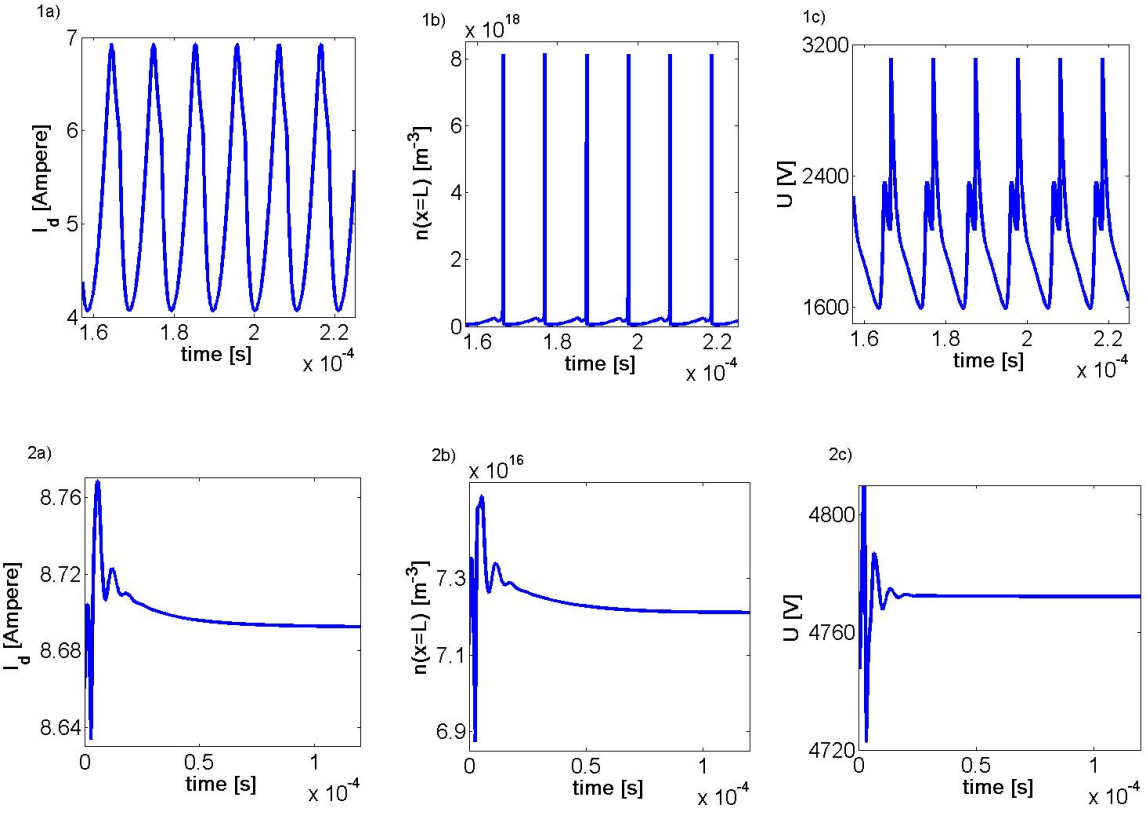

Figure 5.5: Time evolutions of (a) $I_d(t)$, (b) $n(x = L, t)$, (c) $U(t)$ in the (1) periodic regime and the (2) stable regime.

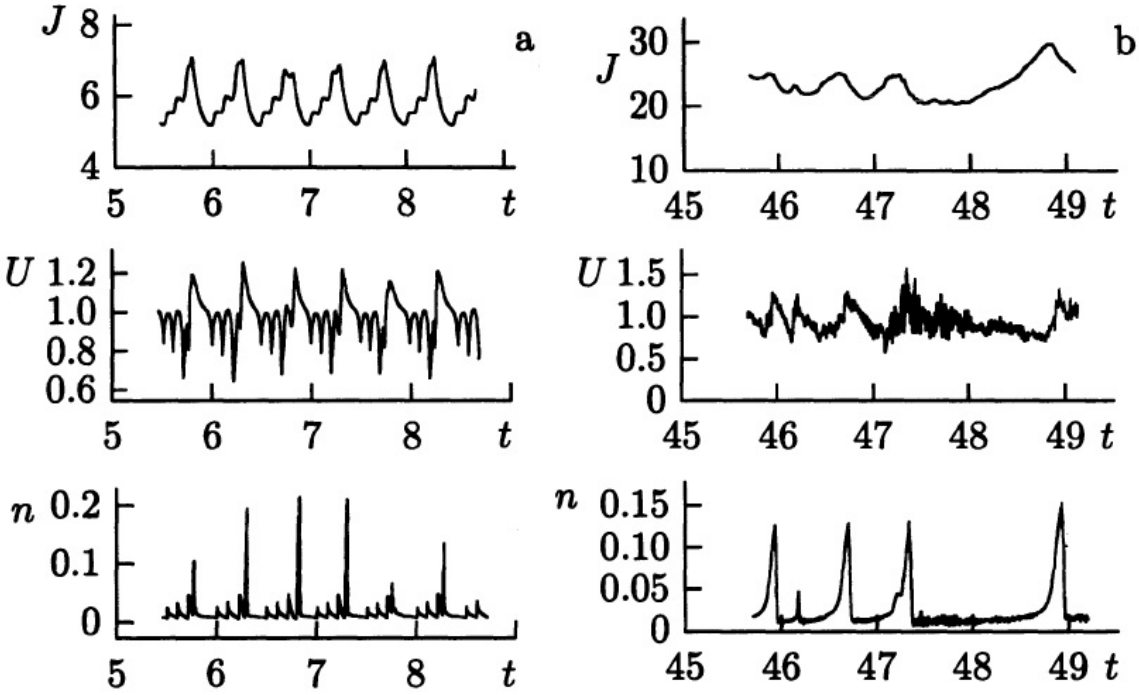

Figure 5.6: Oscillograms of the discharge current, the channel voltage, and the ion density at the channel exit, changing the parameter χ. (a) Periodic oscillations ($\chi = 45$), (b) A non-periodic case ($\chi = 175$) [23].

5.2 Hybrid model

5.2.1 Stationary solution

The stationary equations of the hybrid model are

$$v\frac{\partial \hat{f}}{\partial \hat{x}} + \mu E\frac{\partial \hat{f}}{\partial v} = \hat{\beta}(T)\nu\hat{n}\hat{n}_a\delta(\hat{v} - \hat{v}_a), \tag{5.18}$$

$$\hat{v}_a\frac{\partial \hat{n}_a}{\partial \hat{x}} = -\hat{\beta}(T)\nu\hat{n}\hat{n}_a, \tag{5.19}$$

$$\frac{5}{2}\frac{\partial \hat{n}\hat{v}_e\hat{T}}{\partial \hat{x}} = \kappa\left(\frac{\partial}{\partial \hat{x}}\frac{\hat{T}}{\hat{B}}\frac{\partial \hat{T}}{\partial \hat{x}}\right) + \frac{\zeta}{\chi}\hat{j}_e\hat{E} - \hat{\alpha}\hat{\beta}(T)\nu\hat{n}_a\hat{n}, \tag{5.20}$$

$$\hat{E} = [\hat{B}(\hat{x})]^2(\hat{J} - \chi\hat{n}\hat{v}),$$

$$\hat{J} = \frac{1}{r}\left(1 - \int_0^1 \hat{E}d\hat{x}\right).$$

Again, let's remove the ˆ notation on the non-dimensional variables and denote the RHS of Eq. 5.18 by S. In the hybrid model, as the electric field may change sign locally throughout the iterations, stationary Vlasov equation (Eq. 5.18) is solved using the first order upwind method [32] in order to have numerically stable algorithm.

The Eq. 5.18 is discretized as shown below:

$$f_{i+1,j} = f_{i,j} - \frac{\mu E_i}{v_j}(f_{i,j} - f_{i,j-1})\frac{(\Delta x)_i}{\Delta v} + \frac{S_i(\Delta x)_i}{v_j}, \text{ if } E_i \geq 0,$$

and

$$f_{i+1,j} = f_{i,j} - \frac{\mu E_i}{v_j}(f_{i,j+1} - f_{i,j})\frac{(\Delta x)_i}{\Delta v} + \frac{S_i(\Delta x)_i}{v_j}, \text{ if } E_i < 0.$$

Here

$$S_i = \nu\beta(T)n_i n_{ai}\delta(v_i - v_a). \tag{5.21}$$

Since the electric field grows sharply toward the channel exit, the uniform grid previously used does not yield a converging solution. Instead a non-uniform grid is utilized with decreasing step sizes toward the channel exit, determined according to CFL condition:

$$\Delta x = C\frac{\Delta v\ min(v)}{\mu\ |E(x)|}, \tag{5.22}$$

where $min(v) = \Delta v$ in the velocity space and $C \leq 1$.

The mean values of ion density and velocity are calculated by integrating the ion VDF. The velocity domain should be chosen sufficiently large so that these macroscopic quantities are properly calculated. Therefore, the maximum velocity in VDF is set to one and half of the v_{ex} which is the maximum value of the stationary ion velocity profile in the fluid model. For the velocity space, a uniform grid with 300 nodes is used, which provides a fine enough resolution for the ion VDF.

As in the fluid model, J is found iteratively. But in order to increase stability, a relaxation scheme for J is implemented such that $J^{corrected} = \phi J^{new} + (1-\phi)J^{old}$ with parameter ϕ between 0 and 1).

Grouping the derivatives of T on one side, the electron energy equation (Eq. 5.20) can be rewritten as

$$\frac{\partial}{\partial x}\left(\kappa_0 \frac{T}{B}\frac{\partial T}{\partial x}\right) - \frac{5}{2} n v_e \frac{\partial T}{\partial x} = \frac{5}{2} T \frac{\partial n v_e}{\partial x} - \frac{\zeta j_e E}{\chi} + \alpha\nu\beta(T) n n_a. \tag{5.23}$$

Boundary value problem for this second order non-linear differential equation can be solved by using the tridiagonal matrix algorithm (TDMA) [32]. However, we solved this equation by reducing it to two first order equations and using the Euler method. Let's denote the RHS by S and $\partial T/\partial x$ by T'. Then, we get

$$\frac{\partial T'}{\partial x} = \left[\frac{S + \frac{5}{2} n v_e}{\kappa_0} T' - \frac{(T')^2}{B} + \frac{T' T}{B^2}\frac{\partial B}{\partial x}\right]\frac{B}{T}, \qquad \frac{\partial T}{\partial x} = T', \tag{5.24}$$

with the boundary conditions $T(1) = 1$ and $T'(0) = 0$.

First, S_i is calculated at each grid point.

$$S_i = \frac{5}{2} T_i \frac{n_{i+1} v_{ei+1} - n_{i-1} v_{ei-1}}{2\Delta x} - \frac{j_{ei} E_i \zeta}{\chi} + \alpha\nu\beta T_i n_i n_{ai}. \tag{5.25}$$

Then, T_i and T'_{i+1} are evaluated at each grid point as follows:

$$T_i = T_{i-1} + T'_i \Delta x. \tag{5.26}$$

$$T'_{i+1} = T'_i + \Delta x \frac{B(x_i)}{T_i}\left[\frac{S_i + \frac{5}{2} n_i v_{ei}}{\kappa_0} T'_i - \frac{(T'_i)^2}{B(x_i)} + \frac{T'_i T_i}{[B(x_i)]^2}\frac{B(x_{i+1}) - B(x_{i-1})}{2\Delta x}\right]. \tag{5.27}$$

Using the initial estimation of T and T', T is calculated at each grid point from Eq. 5.26. Then, T' is computed from Eq. 5.27 using the updated values of T. This process is repeated until T converges.

Figure 5.7 shows the axial profiles of the main plasma variables in the thruster discharge channel. When the results of the fluid and the hybrid models are compared, it is seen that the electric field and mean ion velocity profiles are nearly the same. The ion mean velocity reaches $\approx 10\ v_0$ at the channel exit. On the other hand, the ionization takes places closer to the anode in the hybrid model. The neutral atoms are depleted before $x/L \simeq 0.2$. The electron temperature varies only slightly. The temperatures near the anode surface are found

to be higher than expected. Consequently, near the channel base ionization rate parameter is higher in the hybrid model than in the fluid model. Therefore, ionization region shifts slightly to the left in the hybrid case. The electron velocity increases near the anode and reaches $\approx 10 \times v_0$. In Fig. 5.8, the stationary velocity distribution function (VDF) of ions is illustrated, where x,y and z axes correspond to dimensionless velocity, position and VDF.

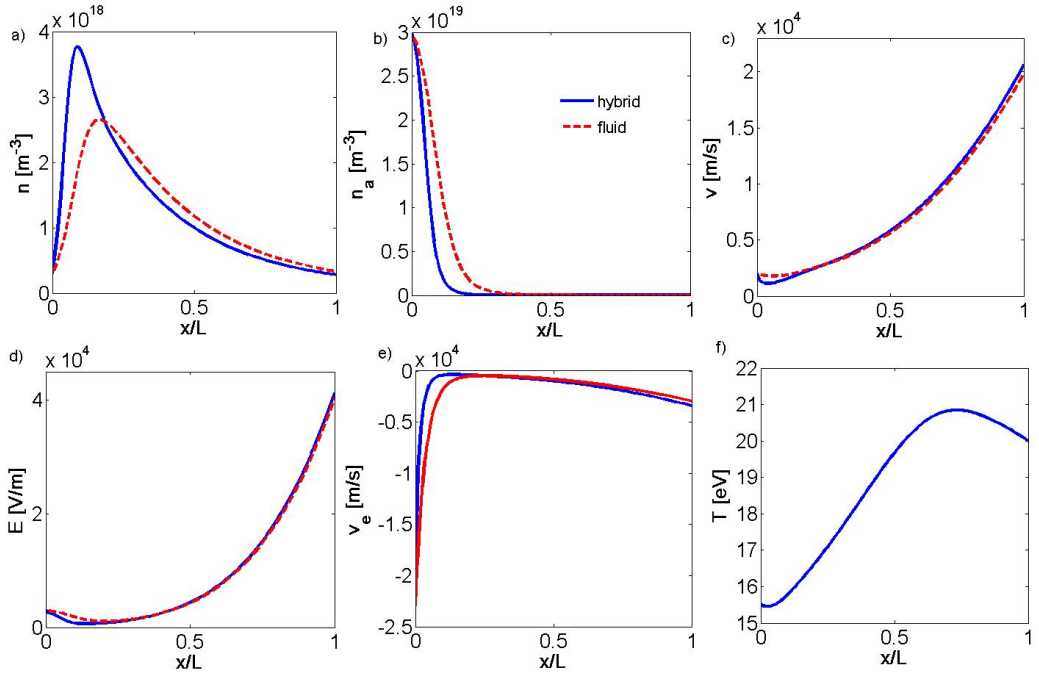

Figure 5.7: Spatial profiles of the main plasma variables in the discharge channel obtained for fluid and hybrid models: (a) ion number density , (b) neutral atom number density, (c) ion velocity, (d) electric field, (e) electron velocity, (f) electron temperature.

5.2.2 Transient solution

As in the fluid model, taking the stationary profiles as initial conditions, time dependent solutions are computed. The time-dependent Vlasov equation involves both position and velocity derivatives. The position derivative at the i^{th} and j^{th} grid point, $(\partial_x f)_{i,j}$ is evaluated by the backward difference:

$$(\partial_x f)_{i,j} = \frac{f_{i,j} - f_{i-1,j}}{\Delta x}.$$

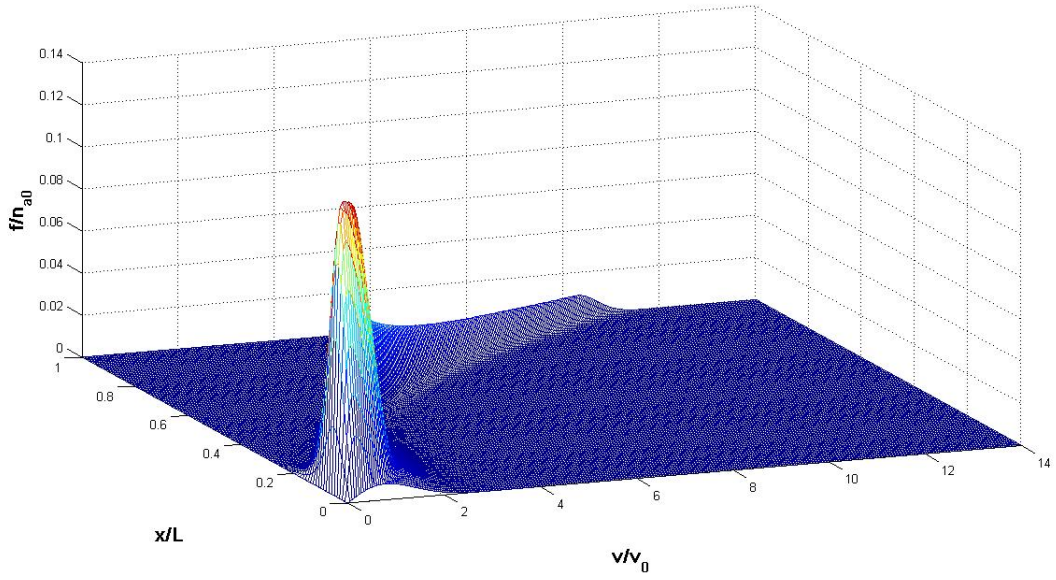

Figure 5.8: Stationary velocity distribution function of ions.

As the electric field may change sign at some locations, the velocity derivative at the i^{th} and j^{th} grid point, $(\partial_v f)_{i,j}$ is evaluated by the upwind scheme:

$$(\partial_v f)_{i,j} = \frac{f_{i,j+1} - f_{i,j}}{\Delta v}, \text{ if } E_i < 0,$$

$$(\partial_v f)_{i,j} = \frac{f_{i,j} - f_{i,j-1}}{\Delta v}, \text{ if } E_i \geq 0,$$

so that

$$f_{i,j}^{k+1} = f_{i,j}^{k} + \Delta t[S_{i,j}^{k} - v_j^k(\partial_x f)_{i,j}^{k} - \nu E_i^k(\partial_v f)_{i,j}^{k}]. \tag{5.28}$$

The time step is determined according to CFL condition:

$$\Delta t = min\left(\frac{C\Delta x}{max(v)}, \frac{C\Delta v}{\mu\ max(|E|)}\right), \quad C \leq 1. \tag{5.29}$$

n_a, E and J are evaluated as in the fluid model from Eq. 5.15, 5.16 and 5.17, respectively. It is assumed that the electron energy is steady in the time scale of ion transport and the time derivative term in the electron energy equation is neglected [3, 15]. Therefore, the electron temperature is calculated by solving the stationary electron energy equation as in the previous section.

Figure 5.9 shows the change of the axial profiles of the ion number density and velocity with time. Contrary to the stationary solution, the profiles of the

transient solution are not monotonic but have some peaks and dips. Obviously, the peaks and dips of the ion number density profiles correspond to the dips and peaks of the ion mean velocity profiles, respectively. The first peaks of the profiles appear in the ionization region. Their amplitude reach the maximum and then they propagate along the channel to right (toward the channel exit) conserving their shape but decreasing their amplitude. As an ion density peak approaches the channel exit, a new one appears in the ionization region and the same process repeats.

Figure 5.10 demonstrates the time dependent behavior of the discharge current $I_d(t)$, the channel voltage $U(t)$ and the ion number density n at the channel exit ($x = L$) for the input parameters $\dot{m} = 3.25$ mg/s and $U_0 = 300$ V. Despite the irregular oscillations of these variables for the same input parameters in the fluid model, the hybrid model yielded periodic oscillations with the main period of $\tau = 50$ μs. This is due to the fact that transitions from stable to periodic and from periodic to aperiodic regimes occur at lower discharge voltages in the hybrid model than in the fluid model. Therefore, while a discharge voltage value of practical interest commonly used on thrusters such as (300 V) falls into chaotic regime in the fluid model, it remains within the periodic regime in the hybrid model. Thus, the hybrid model turns out to be more stable than the fluid model [23]. The oscillation frequency, calculated as 20 kHz for $U_0 = 300$ V, agrees with the results in [3] where frequencies are found to be $15 - 22$ kHz for the voltage range of $200 - 350$ V and with the data taken during tests at NASA/GRC (adopted from [10]) shown in Fig. 5.11.

In Hall thruster operation, different modes of oscillations are observed. The longitudinal oscillation mode with frequencies in the range of $10 - 100$ kHz and which is characterized by strong discharge current oscillations is often referred to as the *breathing mode* [27]. These low-frequency oscillations are related to ionization instabilities that result from the ionization front propagating irregularly around the circumference of the discharge channel [31]. J.M.Fife proposed a simple physical model for breathing mode oscillations in [20]. Linearizing ion and neutral continuity equations around the stationary state, he obtained the

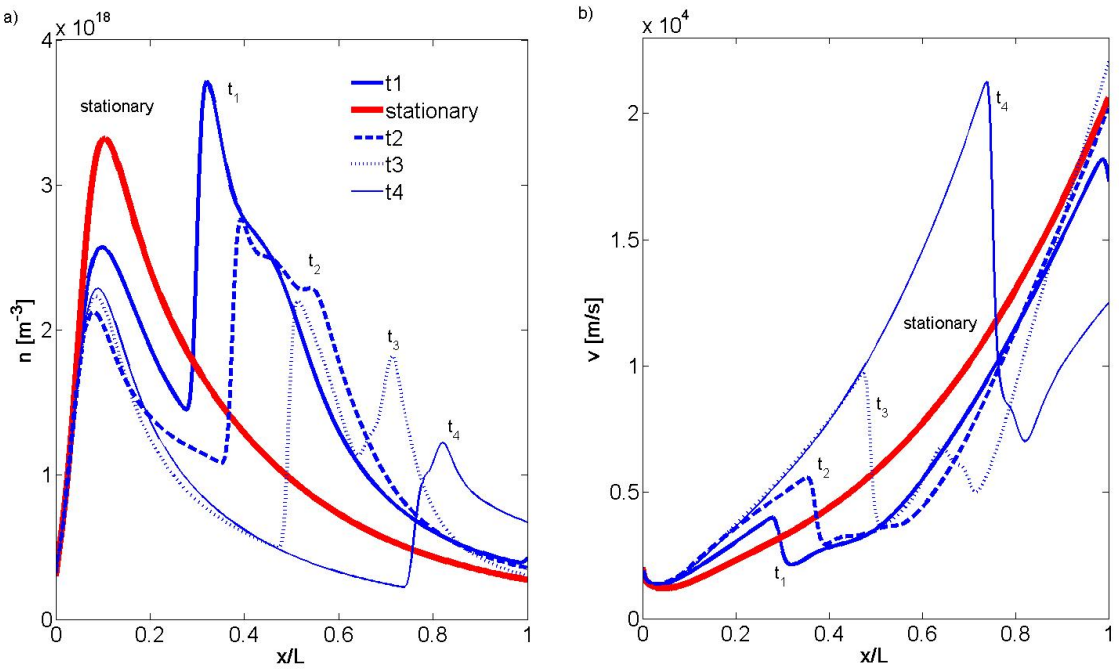

Figure 5.9: Hybrid model spatial profiles of (a) ion number density and (b) ion velocity at different time steps ($t_1 = 0.45$ ms and time intervals are $\Delta t = 2.5$ μs) for $\dot{m} = 3.25$ mg/s and $U_0 = 300$ V.

following expression for the breathing mode frequency, f_B:

$$f_B = \frac{\sqrt{v_i v_a}}{2\pi L_i}, \tag{5.30}$$

where L_i is the characteristic length of the ionization region. For the characteristic ion velocity $v_i = 20000$ m/s, the neutral velocity $v_a = 200$ m/s, and $L_i = 0.02$ m, $f_B = 16$ kHz. This relationship relies on many simplifications, but it does provide correct estimates of the oscillation frequency (about $10 - 30$ kHz).

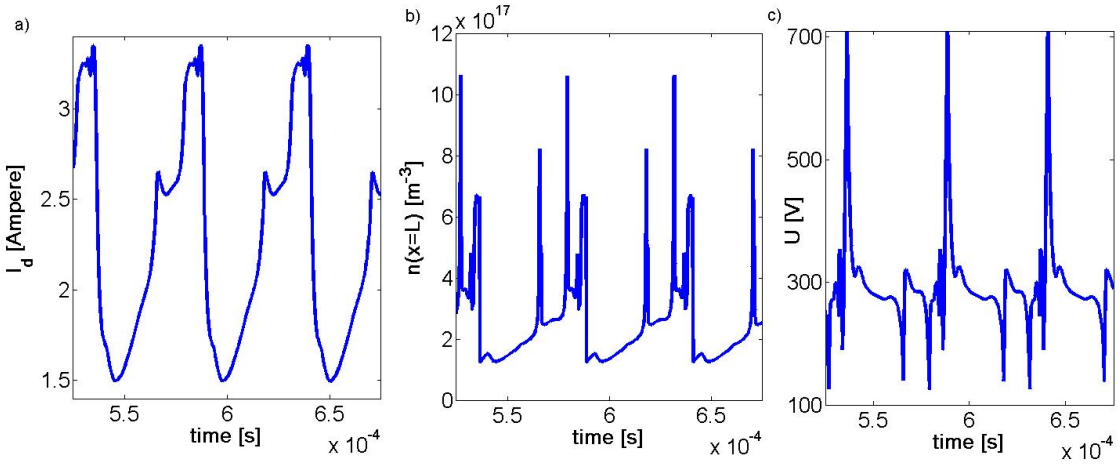

Figure 5.10: Hybrid model time evolutions of (a) $I_d(t)$, (b) $n(x = L, t)$, (c) $U(t)$ for $\dot{m} = 3.25$ mg/s and $U_0 = 300$ V.

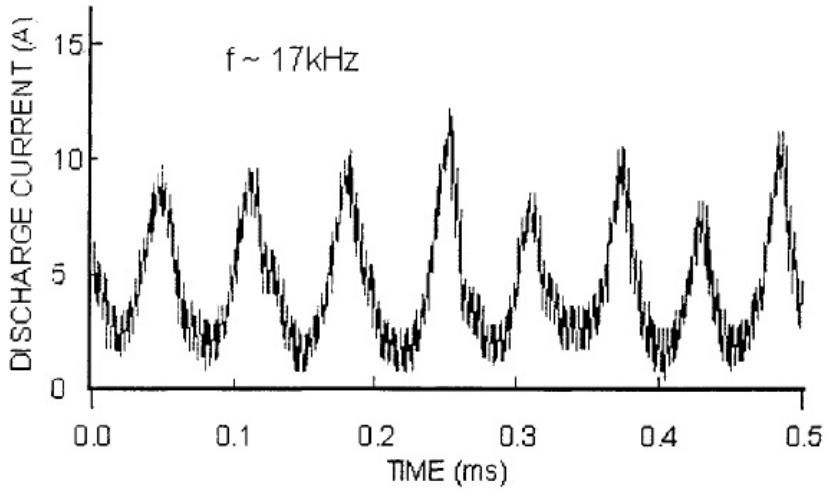

Figure 5.11: Measured evolution of the discharge current for the SPT-100 (data taken during tests at NASA/GRC) [10].

CHAPTER 6

CONCLUSION

6.1 Summary and Conclusions

In this thesis, one-dimensional fluid and hybrid numerical codes are developed in order to study the stationary and evolutionary behaviour of the plasma properties in the discharge channel of a Hall effect thruster. In the fluid model, neutral continuity, ion continuity and momentum equation are solved, while in the hybrid model the fluid equations for ions is replaced by the kinetic Vlasov equation. In both models, electrons are treated as a fluid with a classical conductivity in the direction perpendicular to the magnetic field. The hybrid model additionally includes the electron energy equation.

Stationary profiles of the plasma variables in the discharge channel are obtained from both models. The profiles are found to be close to each other except that the ion density peak is located slightly nearer to the the anode in the hybrid model. Using the values of the plasma properties at the channel exit, the performance parameters of the thruster are predicted.

Using the stationary solutions as initial conditions, time evolution of the plasma variables is investigated. In the time dependent solution, different operating regimes (damped, periodic and aperiodic irregular oscillations about stationary states) are observed as functions of the discharge voltage. The time-dependent simulation predicts the existence of low-frequency discharge oscillations which are typical in Hall thruster operation and accurately estimates the frequency of such oscillations. In general, the results of the numerical code match very well

with those presented in the reference papers [23, 24, 22]. Hence, the accuracy of the numerical methods employed is validated.

It is found out that the convergence of the fluid model code is strongly dependent on the initial estimation of the discharge current. In the hybrid model, however, the code converges for a wider range of the initial discharge current. On the other hand, the fluid model is more efficient in terms of computation time than the hybrid model.

6.2 Future Work

Although the models are based on many approximations, they reproduce qualitatively the basic features of the thruster operation. The quantitative accuracy of the model, however, can be improved by including plasma-wall interaction and considering the effect of secondary electrons emitted by the walls. A weak point of the model is that the electron dynamics is described by the simplified Ohm's Law where the electron conductivity is assumed to have $1/B^2$ dependence. Consequently, electron conductivity is too low in the strong magnetic field region. However, in reality, the electron transport is enhanced by the electron-wall collisions and azimuthal field fluctuations (represented by the Bohm mobility term). Including these effects and electron diffusion term in the model, electron dynamics can be described more accurately.

In this work, it has been assumed that all electron-neutral collisions result in single ionization. However, doubly charged xenon ions and excited xenon atoms are also present in the discharge channel and they should be taken into account.

Finally, a two dimensional model of the discharge channel should be developed in order to investigate the variation of the plasma properties in the radial direction. Effects of plasma-wall interaction on the thruster operation and better description are left to be studied in a more sophisticated model, which is to be developed in a future follow up work.

REFERENCES

[1] Hall thruster schematic. `http://www.laplace.univ-tlse.fr/groupes-de-recherche/groupe-de-recherche-energetique/projets-en-cours/Propulseurs-a-effet-Hall-pour/?lang=en`. [last accessed on 10.08.2014].

[2] J. A. Bittencourt. *Fundamentals of Plasma Physics.* Pergamon Press, 1986.

[3] J.-P. Boeuf and L. Garrigues. Low frequency oscillations in a stationary plasma thruster. *Journal of Applied Physics*, 84:3541–3544, 1998.

[4] C.A.Lentz. Transient one dimensional numerical simulation of hall thrusters. Master's thesis, Massachusetts Institute of Technology, 1993.

[5] E. Y. Choueiri. A critical history of electric propulsion: The first 50 years (1906-1956). *Journal of Propulsion and Power*, 20:193–203, 2004.

[6] I. K. Dan M. Goebel. *Fundamentals of Electric Propulsion: Ion and Hall Thrusters.* JPL Space Science and Technology Series, Wiley.

[7] P. M.-C. E. Ahedo and M. Martinez-Sanchez. One-dimensional model of the plasma flow in a hall thruster. *Physics of Plasmas*, 8:3058–3068, 2001.

[8] F.F.Chen. *Plasma Physics and Controlled Fusion.* Springer, 1974.

[9] M. Hirakawa and Y. Arakawa. Particle simulation of plasma phenomena in hall thrusters. In *24th International Electric Propulsion Conference*, IEPC-1995-164.

[10] R. R. H. Ioannis G. Mikellides, Ira Katz and D. M. Goebel. Hall-effect thruster simulations with 2-d electron transport and hydrodynamic ions. In *31th International Electric Propulsion Conference*, IEPC-2009-114.

[11] J. J. J. Szabo. *Fully Kinetic Modeling of a Hall Thruster.* PhD thesis, Massachusetts Institute of Technology, Department of Aeronautics and Astronautics, 2001.

[12] J.P.Luna. *Modélisation et diagnostics d'un propulseur à effet Hall.* PhD thesis, l'Université de Toulouse-Paul Sabatier, 2008.

[13] J.W.Koo. *Hybrid PIC-MCC Computational Modeling of Hall Thrusters.* PhD thesis, The University of Michigan, 2005.

[14] M. L. R. W. K. Kwon and D. N. Mavris. Self-consistent, one-dimensional analysis of the hall effect thruster. *Plasma Sources Science And Technology*, 20, 2011.

[15] K.Hara and I. D. Boyd. Low frequency oscillation analysis of a hall thruster using a one-dimensional hybrid-direct kinetic simulation. In *33nd International Electric Propulsion Conference*, IEPC-2013-266.

[16] K.Komurasaki and Y.Arakawa. Low frequency oscillations in a stationary plasma thruster. *Journal of Propulsion and Power*, 11:1317–1323, 1995.

[17] J. B. L. Garrigues G. J. M. Hagelaar and J.-P. Boeuf. Two-dimensional model of a stationary plasma thruster. *Journal of Applied Physics*, 91:5592–5598, 2002.

[18] J. E. P. M. Martinez-Sanchez. Spacecraft electric propulsion-an overview. *Journal of Propulsion and Power*, 14:688–699, 1998.

[19] MATLAB. *version 7.10.0 (R2010a)*. The MathWorks Inc., Natick, Massachusetts, 2010.

[20] M.Fife. *Hybrid-PIC Modeling and Electrostatic Probe Survey of Hall Thrusters*. PhD thesis, Massachusetts Institute of Technology, Department of Aeronautics and Astronautics, 1998.

[21] A. I. Morozov. *Vvedenie v plazmodinamiku*. Fizmatlit, 2008.

[22] A. I. Morozov and V. V. Savelyev. One-dimensional hybrid model of a stationary plasma thruster. *Plasma Physics Reports*, 26:3541–3544, 1998.

[23] A. I. Morozov and V. V. Savelyev. Fundamentals of stationary plasma thruster theory. *Reviews of Plasma Physics*, 21:203–391, 2000.

[24] A. I. Morozov and V. V. Savelyev. One-dimensional hydrodynamic model of the atom and ion dynamics in a stationary plasma thruster. *Plasma Physics Reports*, 26:875–880, 2000.

[25] A. O.A.Gorshkov, V.A.Muravlev. *Khollovskie i ionnye plazmennye dvigateli dlya kosmicheskikh apparatov*. Mashinostroyennie, 2008.

[26] S. Roy and B. P. Pandey. Development of a finite element based hall thruster model for sputter yield prediction. In *27th International Electric Propulsion Conference*, Pasadena, CA,.

[27] S.Barral. *Numerical studies of Hall thrusters based on fluid equations for plasma*. PhD thesis, Institute of Fundamental Technological Research Polish Academy of Sciences, 2003.

[28] A. A. S. Sergey V. Irishkov, Oleg A. Gorshkov. Fully kinetic modeling of low-power hall thrusters. In *29th International Electric Propulsion Conference*, IEPC-2005-035.

[29] F. Taccogna and P. Minelli. Three-dimensional fully kinetic particle-in-cell model of hall-effect thruster. In *32nd International Electric Propulsion Conference*, IEPC-2011-088.

[30] V. M. A. S. V. Kim, K.N. Kozubsky. History of the hall thrusters development in ussr. In *30th International Electric Propulsion Conference, Florence, Italy, September 17-20, 2007, IEPC-2007-142*, 2007.

[31] H. R. K. V. V. Zhurin and R. S. Robinson. Physics of closed drift thrusters. *Plasma Sources Science and Technology*, 8:R1–R20, 1999.

[32] J. W.Hundsdorfer. *Numerical Solution of Time-Dependent Advection-Diffusion-Reaction Equations*. Springer, 2003.

APPENDIX A

IONIZATION REACTION RATE COEFFICIENT

Ionization reaction rate coefficient β (which was denoted by $\langle \sigma_i v_e \rangle$ in Sec. 2.6) for xenon is calculated from ionization cross-section data averaged over a Maxwellian electron distribution (See Appendix E in [6]). In the graph below, the ionization rate coefficient, β, is plotted as a function of the electron temperature, where T_{eV} is in eV.

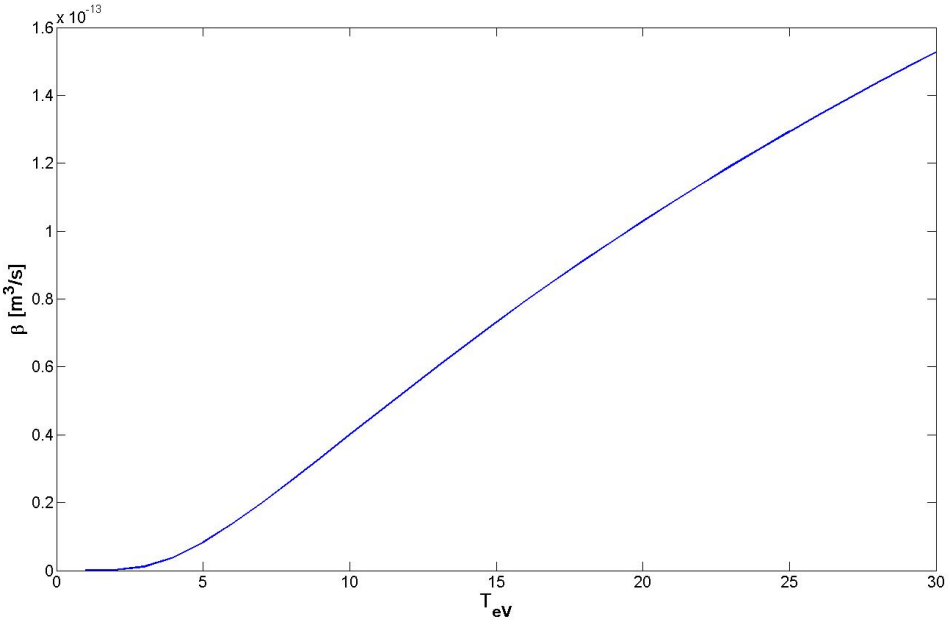

Figure A.1: Ionization reaction rate coefficient versus the electron temperature in eV